

UNIVERSIDADE FEDERAL DE SÃO CARLOS
CENTRO DE CIÊNCIAS EXATAS E DE TECNOLOGIA
DEPARTAMENTO DE QUÍMICA
PROGRAMA DE PÓS-GRADUAÇÃO EM QUÍMICA

Materiais híbridos condutores baseados em grafeno/polímero visando aplicações em monitoramento e remediação de poluentes ambientais

Murilo Henrique Moreira Facure*

Dissertação apresentada como parte dos requisitos para obtenção do título de MESTRE EM QUÍMICA, área de concentração: FÍSICO-QUÍMICA.

Orientador: Dr. Daniel Souza Corrêa

***Bolsista: FAPESP**

São Carlos, SP

2018

UNIVERSIDADE FEDERAL DE SÃO CARLOS
CENTRO DE CIÊNCIAS EXATAS E DE TECNOLOGIA
DEPARTAMENTO DE QUÍMICA
PROGRAMA DE PÓS-GRADUAÇÃO EM QUÍMICA

**Conducting hybrid materials based on graphene/polymer
aiming at applications in monitoring and remediation of
environmental pollutants**

Murilo Henrique Moreira Facure*

Dissertation presented as a part of
the requirements to obtain
MASTER'S DEGREE in
SCIENCES, concentration area:
PHYSICAL CHEMISTRY.

Advisor: Dr. Daniel Souza Corrêa

***Scholarship: FAPESP**

**São Carlos, SP
2018**



UNIVERSIDADE FEDERAL DE SÃO CARLOS

Centro de Ciências Exatas e de Tecnologia
Programa de Pós-Graduação em Química

Folha de Aprovação

Assinaturas dos membros da comissão examinadora que avaliou e aprovou a Defesa de Dissertação de Mestrado do candidato Munio Henrique Moreira Fagure, realizada em 23/10/2018:

A handwritten signature in black ink, appearing to read 'Daniel Souza Corrêa', with a large, stylized initial 'DC' to the right.

Prof. Dr. Daniel Souza Corrêa
EMBRAPA

A handwritten signature in black ink, appearing to read 'Sandra Antêtu Cruz', with a long horizontal stroke extending to the right.

Profa. Dra. Sandra Antêtu Cruz
UFSCar

A handwritten signature in black ink, appearing to read 'Flavio Makoto Shimizu', with a long horizontal stroke extending to the right.

Prof. Dr. Flavio Makoto Shimizu
CNPEM

Este trabalho é dedicado aos meus pais e aos meus irmãos.

AGRADECIMENTOS

Ao Dr. Daniel Souza Corrêa pelas portas abertas, pela dedicada, enriquecedora e valiosa orientação, pelos bons exemplos e confiança.

Aos parceiros nos trabalhos desenvolvidos nesse período, especialmente à Luiza A. Mercante pela inestimável colaboração e pela contribuição no meu desenvolvimento científico.

Aos membros da banca pela disposição e colaboração.

Aos colegas de grupo pelas contribuições na realização deste trabalho e por tornarem o dia a dia muito mais agradável.

À Embrapa Instrumentação pela estrutura disponibilizada e a todo o pessoal de suporte à pesquisa pelo incansável e indispensável auxílio, facilitando todo o processo.

À FAPESP (Processo Nº 2015/13140-0) pela bolsa de mestrado concedida e às demais agências de fomento (CNPq e CAPES) pelo suporte financeiro e pelo provimento de excelentes condições para a realização deste trabalho.

O presente trabalho foi realizado com apoio da Coordenação de Aperfeiçoamento de Pessoal de Nível Superior - Brasil (CAPES) - Código de Financiamento 001.

Ao Programa de Pós-Graduação em Química da Universidade Federal de São Carlos (PPGQ-UFSCar).

Ao LNNano-CNPEM pelo suporte e por proporcionar a fabricação dos eletrodos utilizados.

Ao Laboratório de Caracterização Estrutural (LCE) do Departamento de Engenharia de Materiais da UFSCar, onde foram obtidas imagens enriquecedoras para este trabalho.

Aos novos amigos de São Carlos, da casa, da brasa, da bola, do prato e do copo. Aos velhos amigos de Uberaba.

Aos irmãos de sangue e aos de coração pelos encontros, sorrisos, pelo apoio e otimismo.

Aos maiores e eternos amores pelo amor infinito.

AUTHOR'S PUBLICATIONS

1. FACURE, M. H. M.; MERCANTE, L. A.; MATTOSO, L. H. C.; CORREA, D. S. Detection of trace levels of organophosphate pesticides using an electronic tongue based on graphene hybrid nanocomposites. *Talanta*. **2017**, 167, 59-66.
2. MERCANTE, L. A.; FACURE, M. H. M.; LOCILENTO, D. A.; SANFELICE, R. C.; MIGLIORINI, F. L.; MATTOSO, L. H. C.; CORREA, D. S. Solution blow spun PMMA nanofibers wrapped with reduced graphene oxide as an efficient dye adsorbent *New J. Chem.* **2017**, 41, 9087-9094.
3. MERCANTE, L. A.; FACURE, M. H. M.; SANFELICE, R. C.; MIGLIORINI, F. L.; MATTOSO, L. H. C.; CORREA, D. S. One-pot preparation of PEDOT:PSS-reduced graphene decorated with Au nanoparticles for enzymatic electrochemical sensing of H₂O₂. *Applied Surface Science*. **2017**, 407, 162–170.
4. PAULA, K. T.; GAÁL, G.; ALMEIDA, G. F. B.; ANDRADE, M. B.; FACURE, M. H. M.; CORREA, D. S.; RIUL, A.; RODRIGUES, V.; MENDONÇA, C. R. Femtosecond laser micromachining of polylactic acid/graphene composites for designing interdigitated microelectrodes for sensor applications. *Optics and Laser Technology* **2018**, 101, 74-79.
5. PAVINATTO, A.; MERCANTE, L. A.; FACURE, M. H. M.; PENA, R. B.; SANFELICE, R. C.; MATTOSO, L. H. C.; CORREA, D. S. Ultrasensitive biosensor based on polyvinylpyrrolidone/chitosan/reduced graphene oxide electrospun nanofibers for 17 α – Ethinylestradiol electrochemical detection. *Applied Surface Science*. **2018**, 458, 431–437.

LIST OF FIGURES

FIGURE 1.1.1: Graphene can be wrapped up into 0D fullerenes, rolled into 1D nanotubes or stacked into 3D graphite. (Reprinted with permission from Geim <i>et. al.</i> ⁴)	2
FIGURE 1.1.2: Schematic representation of the route used to obtain graphene-based materials and the models of a graphene oxide and a reduced graphene oxide sheet. (Figure adapted from Compton <i>et. al.</i> ¹⁹).....	3
FIGURE 1.2.1: Schematic representation of the apparatus usually used in an impedimetric e-tongue. (Reprinted with permission from Riul <i>et. al.</i> ⁵⁴).....	8
FIGURE 3.3.1: Schematic illustration (i-ii) of the impedimetric e-tongue system based on graphene hybrid nanocomposites for detection of trace levels of OPs pesticides. (iii) PCA was the statistical technique used to treat the electrical resistance data collected by the e-tongue. (Reprinted with permission from Facure <i>et. al.</i> ⁸⁴)	20
FIGURE 3.4.1: FTIR spectra of rGO (i), PPy-rGO (ii), PEDOT:PSS-rGO (iii) and PEDOT:PSS-rGO-AuNPs (iv). (Reprinted with permission from Facure <i>et. al.</i> ⁸⁴).....	22
FIGURE 3.4.2: STEM images of (A) rGO, (B) PPy-rGO, (C), PEDOT:PSS-rGO, (D) PEDOT:PSS-rGO-AuNPs, (E) histogram of size distribution of gold nanoparticles and (F) EDX spectra of rGO (black), PPy-rGO (green), PEDOT:PSS-rGO (blue) and PEDOT:PSS-rGO-AuNPs (red). (Reprinted with permission from Facure <i>et. al.</i> ⁸⁴) ...	23
FIGURE 3.4.3: Resistance versus frequency data for each sensing unit in PBS buffer solution (0.1 mol L ⁻¹ , pH 7.0). (Reprinted with permission from Facure <i>et. al.</i> ⁸⁴)	24
FIGURE 3.4.4: PCA plots for the electrical resistance responses (experimental data collected with the electronic tongue) at 100 Hz for the analysis of malathion (A) and cadusafos (B) diluted solutions. (Reprinted with permission from Facure <i>et. al.</i> ⁸⁴)....	26
FIGURE 3.4.5: PCA plot for the electrical resistance responses (experimental data collected with the electronic tongue) at 100 Hz for the analysis of malathion and cadusafos solutions. (Reprinted with permission from Facure <i>et. al.</i> ⁸⁴).....	27
FIGURE 3.4.6: PC1 average values versus the concentration of malathion (A) and cadusafos (B) and the respective linear regression. (Reprinted with permission from Facure <i>et. al.</i> ⁸⁴).....	28
FIGURE 3.4.7: PCA plot for the electrical resistance responses (experimental data collected with the electronic tongue) at 100 Hz for the analysis of malathion and cadusafos solutions prepared with PBS buffer solution and tap water (real samples). (Reprinted with permission from Facure <i>et. al.</i> ⁸⁴)	30
FIGURE 4.3.1: Sketch of the steps involved in the preparation of PMMA-rGO composite nanofibers: (A) solution blow spinning PMMA nanofibers and (B) surface modification: (i) plasma treatment, (ii) GO adsorption and (iii) GO reduction. (C) Scheme of the decontamination process of MB-containing water using the developed composite nanofibers. (Reprinted with permission from Mercante <i>et. al.</i> ¹³⁰)	36

FIGURE 4.4.1: SEM images of (a) PMMA nanofibers, (b) PMMA-GO nanofibers without and (c) with plasma treatment. (d) Magnified image of panel (c). (Reprinted with permission from Mercante <i>et. al.</i> ¹³⁰).....	39
FIGURE 4.4.2: Photographs of a water droplet on PMMA fibers (a) before and (b) after plasma treatment. (c) FTIR spectra of pure PMMA (i), PMMA-GO (ii), PMMA-rGO (iii) and PMMA-rGO@MB (iv) nanofibers. (Reprinted with permission from Mercante <i>et. al.</i> ¹³⁰)	40
FIGURE 4.4.3: (a) Photographs of PMMA, PMMA-GO, PMMA-rGO and PMMA-rGO@MB nanofiber mats. (b) UV-Vis absorption spectra of MB aqueous solution in the presence of a PMMA-rGO membrane at different time intervals and (c) comparison of the extent of decontamination when using PMMA-rGO, with respect to those obtained with PMMA and PMMA-GO nanofiber mats after 60 min. Error bars indicate the standard deviation of the three measurements. (Reprinted with permission from Mercante <i>et. al.</i> ¹³⁰)	42
FIGURE 4.4.4: (a) pseudo-first order and (b) pseudo-second order plots for adsorption of MB on PMMA-rGO nanofiber membrane. (Reprinted with permission from Mercante <i>et. al.</i> ¹³⁰)	44
FIGURE 4.4.5: The linearized (a) Langmuir and (b) Freundlich isotherms for adsorption of MB on PMMA-rGO nanofiber membrane. (Reprinted with permission from Mercante <i>et. al.</i> ¹³⁰)	46
Figure A1: Digital picture (A) and a scheme of the geometrical features of the IDE (B). The fingers have a length (L) of 4 mm and width (w) and distance between fingers (s) of 10 μ m.	59
Figure A2: UV-Vis absorption spectra of: (i) rGO, (ii) PPy-rGO, (iii) PEDOT:PSS-rGO and (iv) PEDOT:PSS-rGO-AuNPs.....	59
Figure A3: Energy-dispersive X-ray (EDX) spectroscopy images illustrating the distribution of the C, O and N elements in the PPy-rGO nanocomposite.	60
Figure B1: SEM images of PMMA-GO nanofibers using distinct adsorption times: (a) 30 min, (b) 1h and (c) 2h.	61
Figure C1: Permission to use the article “Detection of trace levels of organophosphate pesticides using an electronic tongue based on graphene hybrid nanocomposites”. ..	62
Figure C2: Permission to use the article “Solution blow spun PMMA nanofibers wrapped with reduced graphene oxide as an efficient dye adsorbent”.....	63
Figure C3: Permission to use figures from the article “The rise of graphene”.	64
Figure C4: Permission to use figures from the article “Graphene Oxide, Highly Reduced Graphene Oxide, and Graphene: Versatile Building Blocks for Carbon-Based Materials”.....	64
Figure C5: Permission to use figures from the article “Recent advances in electronic tongues”.	65

RESUMO

MATERIAIS HÍBRIDOS CONDUTORES BASEADOS EM GRAFENO/POLÍMERO VISANDO APLICAÇÕES EM MONITORAMENTO E REMEDIAÇÃO DE POLUENTES AMBIENTAIS. O grafeno é um material formado por uma única camada de átomos de carbono arranjados em anéis de seis átomos com hibridização sp^2 . Além de possuir alta sensibilidade à presença de moléculas, o grafeno apresenta outras interessantes características, como alta condutividade elétrica, resistência mecânica e estabilidade química, sendo considerado um material com elevado potencial de aplicação para diversas tecnologias. Neste trabalho, materiais à base de grafeno e polímeros foram produzidos e utilizados como constituintes de unidades sensoriais de uma língua eletrônica na análise de pesticidas organofosforados e também em plataformas para remediação de poluentes baseado na adsorção do corante azul de metileno em solução aquosa. Materiais à base de grafeno foram obtidos através da redução química do óxido de grafeno, sintetizado a partir do método de Hummers modificado. A caracterização físico-química dos materiais foi realizada através das técnicas de espectroscopia de FTIR e absorção UV-vis e a morfologia foi avaliada através de imagens de microscopia eletrônica de varredura por transmissão. As unidades sensoriais da língua eletrônica foram obtidas utilizando o óxido de grafeno reduzido (rGO) e nanocompósitos obtidos através da combinação deste material com os polímeros poli(3,4-etilendioxitiofeno)-poli(estireno sulfonato) (PEDOT:PSS) e polipirrol, além de nanopartículas de ouro. As respostas obtidas foram tratadas através do método de Análise dos Componentes Principais (PCA), as quais mostraram que o sistema se apresentou capaz de discriminar soluções de pesticidas organofosforados em concentrações nanomolares, soluções com misturas destes pesticidas e de amostras reais, apresentando uma relação direta entre as concentrações dos pesticidas e os valores dos componentes principais nos gráficos de PCA. Os materiais possibilitaram a fabricação de unidades sensoriais com elevada área superficial e alta condutividade elétrica, resultando em um sensor de alta sensibilidade. Outra aplicação estudada neste trabalho, foi a produção de um nanocompósito de rGO e nanofibras de polimetilmetacrilato, produzidas pela técnica de fiação por sopro, que foi empregado como plataforma para remediação de poluente, especificamente na adsorção do corante azul de metileno. A adsorção segue uma cinética de pseudo-segunda ordem e o modelo da isoterma de Langmuir. Os resultados sugerem que a performance da membrana produzida se deve ao efeito sinérgico das fortes

interações π - π entre o corante e o rGO combinadas com as propriedades das nanofibras, como alta porosidade e alta área superficial específica.

ABSTRACT

CONDUCTING HYBRID MATERIALS BASED ON GRAPHENE/POLYMER AIMING AT APPLICATIONS IN MONITORING AND REMEDIATION OF ENVIRONMENTAL POLLUTANTS. Graphene is a material composed of a single layer of carbon atoms arranged in rings of six atoms with sp^2 hybridization. Graphene displays a high sensitivity towards several molecules. Additionally, graphene presents other interesting features such as high electrical and thermal conductivity, mechanical strength and chemical stability, being considered a material with high potential for several technological applications. Herein, graphene-based and polymer-based materials were produced and used as constituents of sensing units of an electronic tongue in analyzes of organophosphorus pesticides and in pollutants remediation platforms based on the adsorption of methylene blue dye in aqueous solution. Graphene-based materials were obtained by chemical reduction of graphene oxide, which was synthesized using the modified Hummers method. The materials' physicochemical characterization was performed using Fourier transform infrared (FTIR) and UV–vis absorption spectroscopy and the morphology was analyzed using Scanning Transmission Electron Microscopy (STEM) images. The sensing units of the electronic tongue were obtained by using reduced graphene oxide (rGO) and nanocomposites obtained by the combination of the rGO with poly(3,4-ethylenedioxythiophene)-poly(styrenesulfonate) (PEDOT:PSS), polypyrrole and gold nanoparticles. The data were treated by Principal Component Analysis (PCA). The system was able to discriminate solutions of OP pesticides at nanomolar concentrations, solutions with the mixture of these pesticides and real samples, presenting a direct relationship between the pesticide concentrations and the values of the principal components in the PCA plots. The materials employed provided sensing units with a high specific surface area and high conductivity, yielding the development of a sensor with high sensitivity. In another work, a nanocomposite made of rGO and poly(methylmethacrylate) nanofibers, produced by the Solution Blow Spinning (SBS) technique, was employed in the adsorption of the methylene blue dye. The dye adsorption kinetics and isotherm follow the pseudo-second-order and the Langmuir models, respectively. The results suggest that the adsorption capabilities of the membrane obtained are due to the synergistic effect of the strong π – π stacking interactions between the dye and the rGO combined with the properties of the

electrospun nanofibers, such as high porosity and high-specific surface area per unit mass.

SUMMARY

1. Introduction	1
1.1. Nanomaterials	1
1.2. Electronic Tongue	6
1.3. Adsorption	9
1.4. Solution Blow Spinning.....	11
2. Goals and Overview	13
3. Chapter I: Electronic tongue based on reduced graphene oxide*	14
3.1. Abstract.....	15
3.2. Introduction	15
3.3. Material and methods.....	17
3.4. Results and discussion.....	21
3.5. Conclusion	31
4. Chapter II: PMMA nanofibers modified with reduced graphene oxide as adsorbent*	32
4.1. Abstract.....	33
4.2. Introduction	33
4.3. Experimental	35
4.4. Results and discussion.....	38
4.5. Conclusion	47
5. General Conclusions and Future Perspectives.....	48
6. References.....	49
Appendix A.....	59
Appendix B.....	61
Appendix C.....	62

1.Introduction

1.1.Nanomaterials

Materials that present one or more dimensions in the nanoscale range, *i.e.* between 1 and 100 nm, are classified as nanomaterials.¹ Research about nanomaterials have increased lately, where the miniaturization of devices is highly pursued, leading to lighter, more efficient and stronger gadgets. Once the material's properties are dependent on their dimensions, the physical and chemical properties of a bulk material can be drastically changed when they are reduced to the nanoscale. The surface area/volume ratio increases with decreasing particle size, influencing interfacial, electrical and optical properties of the materials. Therefore, it is clear that studies on nanomaterials and its processes and the development of novel experimental and theoretical techniques, as well as novel technologies based on this sort of materials will lead to major scientific and technological advances.¹⁻³

Graphene

Graphene is a two-dimensional (2D) material consisting of a monolayer of carbon atoms arranged in rings of six atoms with sp^2 hybridization, which is considered the building material for all carbon allotropes, as shown in Fig. 1.1.1.⁴ Until 2004, it was believed that 2D materials would not exist in the free state, when then graphene was obtained by mechanical exfoliation, being the first 2D atomic crystal isolated.^{5,6}

The discovery of graphene enabled the confirmation of the outstanding characteristics predicted for this material. Graphene showed extremely high electron mobility at room temperature, Young's modulus of 1 TPa, strength and very high thermal conductivity, impermeability to gases, chemical stability and the ability to sustain extremely high densities of electric current.⁷

Graphene can be obtained by various methods using relatively simple and cheap laboratory procedures. Liquid phase and thermal exfoliation of graphite are used to produce pristine graphene.^{7,8} Graphite can be exfoliated in a suitable solvent with the aid of sonication⁹ or can be intercalated with small molecules giving rise to graphene. Large-area and uniform graphene films can also be achieved using epitaxial growth or chemical vapor deposition.^{8,10}

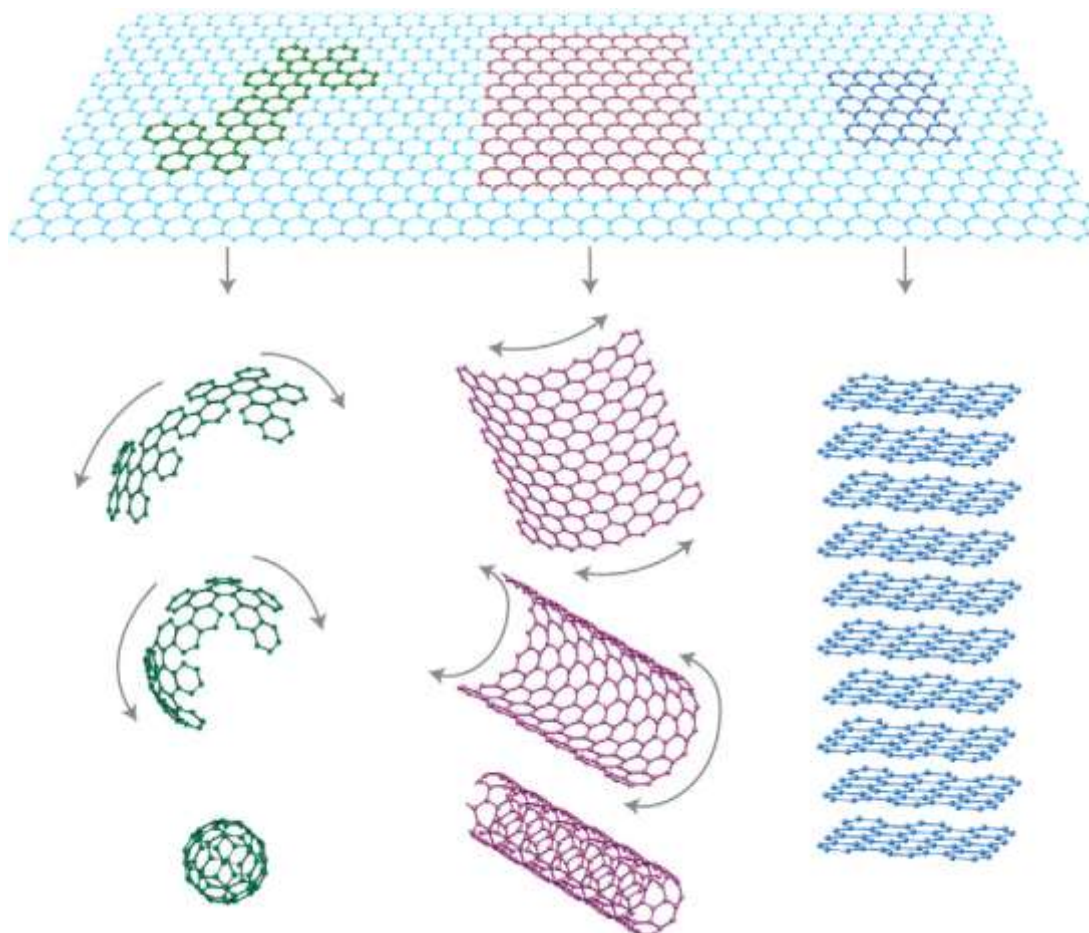


FIGURE 1.1.1: Graphene can be wrapped up into 0D fullerenes, rolled into 1D nanotubes or stacked into 3D graphite. (Reprinted with permission from Geim *et. al.*⁴)

Among many routes,^{9–13} the reduction of graphene oxide (GO) has been widely used to produce graphene-based materials. Although it does not yield pristine graphene, this approach presents some advantages. GO can be easily synthesized using well-established methods and their modifications.^{14–17} GO is characterized as a graphitic monolayer with randomly distributed aromatic regions (sp^2 carbon atoms) and oxygenated aliphatic regions (sp^3 carbon atoms) containing carboxyl, hydroxyl, carbonyl and epoxy groups. The extent of oxidation is quantified by the C:O atomic ratio and is dependent upon the method of synthesis chosen.^{18,19} The use of GO as a precursor material has attracted interest because it can be easily produced from graphite as raw material and can be dispersed in a stable aqueous solution due to its high hydrophilicity. The reduction of GO partly restores the structure and properties of graphene through the removal of oxygen groups, leading to a material denominated as reduced graphene oxide (rGO) that presents similar characteristics when compared

to pristine graphene.¹⁰ The reduction of GO can be accomplished through different approaches, such as thermal and chemical reduction. The method used to synthesize GO and the reduction process used to obtain rGO will lead to different material structures, with different degrees of reduction, defects and functional groups. Since the properties of the final material are dependent on structure, the route used will affect the final performance of the material and the devices that it will compose.^{8,10,20,21} A scheme of the route used in this work is presented in Fig. 1.1.2, as well as the models of the structural backbone of GO and rGO¹⁹.

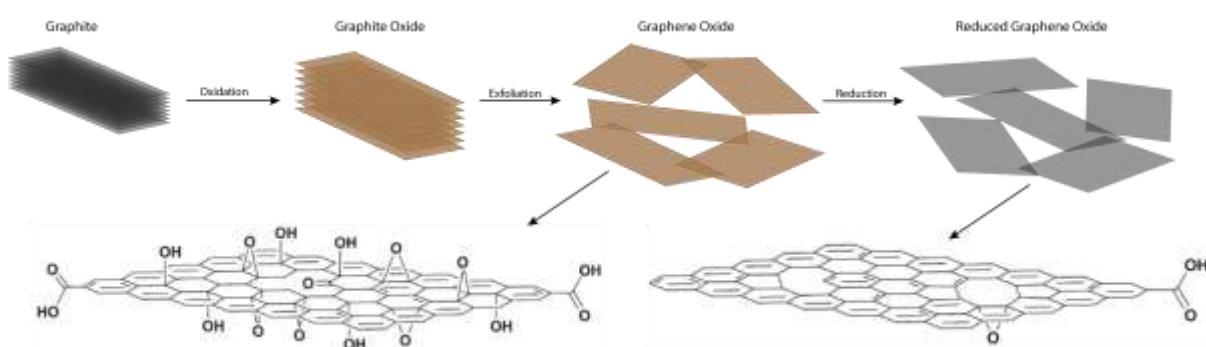


FIGURE 1.1.2: Schematic representation of the route used to obtain graphene-based materials and the models of a graphene oxide and a reduced graphene oxide sheet. (Figure adapted from Compton *et. al.*¹⁹)

Graphene can still be doped or functionalized to modify its characteristics, reaching desired properties and increasing the application possibilities of this material and its based-devices.^{18,22,23} Graphene-based nanocomposites can be developed seeking an enhancement in the mechanical, thermal and electrical properties. Moreover, graphene as well as rGO sheets tend to aggregate irreversibly or restack due the intermolecular van der Waals and π - π interactions between the layers. Such aggregation can be avoided or diminished by the incorporation of small molecules or polymers in graphene sheets. Cationic and anionic species attached to individual layers may increase the stability of graphene dispersions due to electrostatic repulsion. Graphene and its derivative materials can be functionalized with several different materials, with different sizes and characteristics, such as polymers,^{12,24-27} metal or metal oxide nanoparticles,²⁸⁻³¹ quantum dots,^{32,33} biomolecules and others.^{22,23} The modification of GO sheets is usually carried out prior to the reduction

process preventing agglomeration and maintaining the inherent properties of graphene.^{12,19,22} The functionalization of GO sheets is usually achieved in an easy way because of the highly oxygenated surface, in which the functional groups act as active sites in the incorporation of other materials and alter van der Waals forces, making it possible to obtain very stable dispersions of GO in a wide range of organic solvents.^{18,22}

The modification of the graphene framework can be realized by covalent or noncovalent functionalization. The former is characterized by the rehybridization of the sp^2 carbon atoms of the carbon network into the sp^3 configuration. The structural alterations lead to a loss of electronic conjugation and can occur in the end and/or in the surface of the graphene sheet. The latter requires physical adsorption of suitable molecules on the graphene surface, not altering its structure and electronic and mechanical properties. The process can occur through different interactions, such as hydrogen bonding, π - π interactions, van der Waals and electrostatic forces.^{18,22,23}

The huge interest in graphene arose mainly from its outstanding properties and the possibility of obtaining graphene-based materials with distinct characteristics that allow their use in different applications in many fields.^{7,18,22,34} Graphene-based materials have been used in nanoelectronics, drug delivery, supercapacitors, transistors, in the composition of flexible electrodes, as a component in energy materials, in solar and fuel cells, for H_2 storage, in green chemistry, in catalysis, electrocatalysis and photocatalysis.^{7,22,23,27}

The use of graphene in the composition of materials destined to environmental applications has grown notably. Its unique physicochemical properties can give rise to new alternatives and improved technologies to address and solve current environmental challenges. Graphene-based materials have been developed for contaminant monitoring or removal, as well as for water treatment and decontamination.³⁵

Graphene use in sensing and biosensing is particularly interesting because of its characteristics, especially biocompatibility and electronic properties, as well as the fact that the one atom thickness 2D structure leads to the complete exposure of its atoms. Additionally, the presence of a conjugated π bond favors the charge-transfer interactions with analytes, presenting high sensitivity towards molecules.^{27,36} Therefore, graphene is suitable to be applied as the base material of sensors and biosensors in various modes of transduction, from electrical and

electrochemical to optical.³⁴ On the other hand, the use of graphene-based materials as a constituent element in sensing units of an electronic tongue (e-tongue) has not yet been widely reported and explored in scientific works. In this scenario, its use in e-tongues can give rise to more practical, stable and reproducible devices.

In the field of pollutants removal, graphene-based materials may be suitable as an adsorbent for inorganic, organic and gaseous contaminants, presenting inexpensive technological improvements for this area and some advantages in performance over well-established and already explored adsorbent materials.^{35,37,38}

Polymers

Polymers have been widely used combined to graphene in order to obtain functional nanocomposites. Besides resulting in materials with improved physicochemical properties, the association of polymer and graphene can prevent the agglomeration of graphene sheets, improving the solubility and processability of the obtained solution.²⁶ Furthermore, the use of polymers may be interesting in some specific areas, including sensor applications in which the functional groups of the polymer can improve the interaction with the target molecule, considering this interaction with pristine graphene is unfavorable due the absence of hydrophilic groups. However, graphene is important to decrease the electron transfer distance between the active sites of the biomolecules and the electrode area.²² In this context, the use of conducting polymers (CP) is even more interesting because they can maintain the desired electrical characteristics for this sort of application.³⁹

Studies on CP began in the 1970s with the preparation of semiconducting films of poly(acetylene)⁴⁰ and their further doping, which increased the conductivity by 13 orders of magnitude.⁴¹ Since then, the development of the CP field has grown at a very rapid rate due to the possibility of applications into several fields and technologies.^{42,43}

Conducting polymers contain a π -electron conjugation along the polymer backbone responsible for their interesting electrical and optical properties. The electrical conductivity in CP can be explained using concepts of solitons, polarons and bipolarons and it is influenced by a variety of factors including polaron length, the overall chain length, the conjugation length and the charge transfer to adjacent molecules. In order to achieve the conducting property, the polymers have to go through a doping process after which the neutral polymer is converted into a charged

macromolecule. Redox doping, doping without dopant ions and non-redox or protonation doping are examples of the main types of doping process for CPs.^{39,43}

Controlling the structure and morphology of CPs at the nanoscale can lead to improved features not presented by the bulk materials. Conductive polymers are largely used as constituent materials of nanocomposites opening up a wide array of possible combinations to achieve desired physical and chemical properties not possessed by their bulk counterparts. Many of these new characteristics are due to surface structural features and quantum mechanical properties imparted by the nanostructuring process.⁴²

Because of their appealing characteristics, the possibility to control or tailor many of their properties, the wide range of CPs nanocomposites that can be obtained, the different methods available of synthesis, CPs-based materials find applications in many fields. Indeed, the use of CPs have being reported in sensing with the different operating mechanism, including chemical, electrochemical, optical and fluorescence-based (bio)sensors, in sensor arrays, in biomedical applications, in solar cells, in catalysis, as transistors, among others.^{39,42–44}

The choice of the polymer to obtain the graphene-based nanocomposite is of fundamental importance. The use of graphene combined with some polymers has already been explored. The polymer blend poly(3,4-ethylenedioxythiophene)-poly(styrenesulfonate) (PEDOT:PSS) and polypyrrole (PPy) can be associated with graphene-based materials leading to nanocomposites with interesting conducting properties.^{45–49} The polymers can be mixed with GO prior to the chemical reduction, preventing the aggregation of the graphene platelets and giving rise to more stable dispersions.^{27,50}

1.2. Electronic Tongue

The taste system in mammals is composed of taste buds that act as nonspecific receptors, responding to different substances simultaneously. This information is transduced into electric signals and then transmitted to the brain, where the taste is perceived. An electronic tongue (e-tongue) is an analytical instrument for liquid analyses inspired by the biological taste system. An e-tongue is usually composed of a set of nonspecific or low-selective sensing units (array of chemical

sensors) with high stability and cross-sensitivity associated with a suitable pattern recognition method or multivariate calibration tool for data processing.^{51–53} Selectivity is not a compulsory feature because the sensing units are expected to respond in a stable manner to several components of the analyte medium simultaneously, characterizing the global selectivity and cross-sensitivity. Accordingly, for each sample analyzed a fingerprint is obtained. Any slight change in the sample will be detected by the e-tongue, generating a different fingerprint. Thus, e-tongues can be employed in the classification (recognition, identification, discrimination) and quantitative determination of multicomponent and complex solutions, including varied beverages, ethanol/water mixtures, pharmaceutical products and in the monitoring of water quality samples.^{51,54–56}

E-tongues can be based on different methods of detection. The most employed methods use electrochemical measurements, mainly potentiometry, amperometry and voltammetry. These methods have some advantages, e.g. high sensitivity, simple instrumentation and a well-known principle of operation.^{53,54,57} Impedance spectroscopy was first employed for e-tongues in 2002 by Riul *et al.*^{58,59} The impedimetric e-tongue present some advantages when compared to electrochemical methods because it has also high sensitivity, does not require sensing units with electroactive materials or active species in the measuring system and a reference electrode is not required.^{53,54,57} In this method, the sensing units are composed of interdigitated electrodes (IDEs) covered with ultrathin films of different materials and the measurements are carried out varying the frequency and collecting the impedance data. The process and the experimental setup usually employed in impedance spectroscopy measurements are illustrated in Fig. 1.2.1. At low frequencies the response is governed by the double-layer at the electrode/electrolyte interface, while at higher frequencies the geometric capacitance is most relevant. The solution conductance and the effects of the coating material over the electrodes is responsible for the total impedance at intermediate frequencies.^{54,58}

The amount of information generated with the analyzes performed by the system array is usually large, especially when a large number of solutions are studied or when many analyzes are necessary to distinguish very similar samples. Moreover, the data obtained can be complex signals that should be analyzed together to extract useful analytical information. Therefore, it is compulsory to use data processing methods to extract and interpret results from the measurements carried out.^{51,52,54}

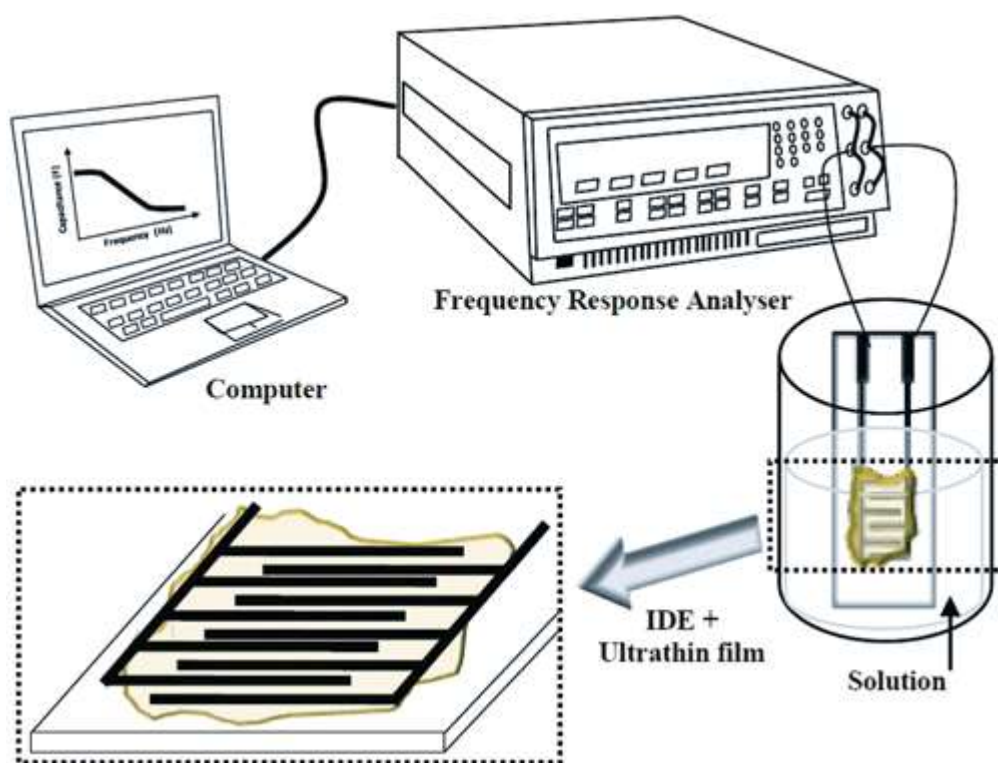


FIGURE 1.2.1: Schematic representation of the apparatus usually used in an impedimetric e-tongue. (Reprinted with permission from Riul *et. al.*⁵⁴)

There are some methods for processing multivariate experimental data employed for e-tongues. Partial least-squares regression (PLS), self-organizing map (SOM), artificial neural networks (AANs) and Principal Component Analyzes (PCA) are often used in this field.^{51,52} PCA is the most used process in the literature for e-tongues.⁵⁴ Through a mathematical algorithm, PCA reduces the dimensionality of the data without loss of information, making a linear combination, creating new directions, the principal components, along which the variation of the data is the highest. The result of the treatment can be visualized through graphics in two or three dimensions, each axis representing a principal component. The graphics are used to assess similarities and differences among samples. In the case of impedimetric e-tongues, the input data is provided as matrices with the electrical responses obtained where rows represent the number of experiments and the columns represent the sensing units used.^{54,60,61}

The choice of the materials to be used in the sensing units of an e-tongue is of primary importance for high performance and should be done considering the

chemical nature of the samples and analytes to be investigated. The sensing units need also to be chemosensitive and respond electrically to minor changes in the liquid to be analyzed. The various possibilities of combining different sensors must lead to complementary and complete information about the analytes.^{53,54,57} Various class of materials has been used in impedimetric e-tongues, including lipidic membranes,^{54,57,62} conducting polymers,^{56,58,59,63,64} oxides,⁵⁵ phthalocyanines,^{56,64} porphyrins⁵⁴ and ruthenium complexes^{59,65}. The use of other materials that have not yet been properly exploited in an electronic tongue can lead to improvements in the performance of such devices. In this scenario, the use of graphene-based materials can lead to an improvement of the sensing capability of new technologies.

1.3.Adsorption

Adsorption is a fast, low-cost, ease of operation and widely applicable alternative for the removal of undesired compounds. It is a spontaneous phenomenon, in which the concentration of a particular component increases at the surface or at the interface between two phases.⁶⁶ The process can occur in solid-liquid, solid-gas, liquid-liquid and liquid-gas systems. The adsorbed component is denominated as adsorbate and the material that retains this component is defined as the adsorbent.^{66,67} Adsorption depends on temperature and on the nature and concentration of the adsorbate. When the process occurs through chemical bonds, it is denominated as chemical adsorption or chemisorption. On the other hand, when the process occurs by van der Waals interaction, it is called as physical adsorption or physisorption and in this case, the forces of attraction are weaker.^{66,68}

Adsorption is also a time-dependent process and for this reason thermodynamics and kinetics studies are of fundamental importance in the acquisition of information about the final equilibrium interfacial energy and the rate of adsorption. While kinetics deals about the rate of changes occurring during the process, thermodynamics gives information about the final state of the system.⁶⁹

The kinetics information collected is important for evaluating the feasibility of the process, the adsorbent efficiency and for the sake of comparison between experimental behavior and the expected one theoretically. Hence, one can better understand the process and find better conditions in order to optimize the results.

The most used models are first order, pseudo-first and pseudo-second order models, in which kinetics equations are proposed in the form of chemical equations to explain the process.^{66,68,69}

Thermodynamics studies, in turn, are commonly realized through adsorption isotherms, regardless of the system interface. The isotherms consist in the fundamental concept in adsorption science and graphically represent the relation between the quantity of adsorbate per mass unit of the adsorbent and the pressure or concentration of the adsorbate in the bulk fluid phase (liquid or gas) at a constant temperature. Through their analyzes important information can be obtained, such as the influence of temperature, the nature of the interactions between adsorbate and adsorbent, the existence of active sites in the adsorbent and the maximum adsorption capacity of the system. Therefore, isotherms help in the selection of suitable adsorbates and in choosing parameters for specific applications.^{68,69} Equilibrium models are used to describe adsorption isotherms. There are some more frequently used models, but no one is generally applicable. Thus, tests are made in order to obtain one model that best fits the experimental data under one set of conditions and can describe the studied process.⁷⁰

The Langmuir model is based on a continuous process of adsorption of molecules onto the surface of the adsorbent and a corresponding desorption of other molecules, therefore, maintaining a zero rate of accumulation at the surface under an equilibrium condition. In this model, it is assumed that: (i) the surface is homogeneous, that is, the adsorption energy is constant over all sites; (ii) the adsorption occurs at localized sites with no interaction between adsorbate molecules and (iii) each site can accommodate only one adsorbate molecule.^{70,71} The Langmuir isotherm is presented in equation 1. It is derived from a solid-gas system, but analogously an isotherm for a solid-liquid system can be derived.

$$q_e = Q^o \frac{bC_e}{1+bC_e} \quad (1)$$

where q_e is the amount of adsorbate per weight unit of adsorbent, Q is the solid phase concentration corresponding to complete coverage of available sites and C_e is the residual liquid phase at equilibrium.^{66,70}

The Freundlich model is an empirical equation (eqn (2)) that can better describe the adsorption equilibrium data, assuming heterogeneous surfaces and

multilayer adsorption. However, at low pressure this equation does not present a proper Henry's law behavior and at high temperature the isotherm does not have a finite limit. Therefore, the Freundlich model should be used in situations that do not present such limitations.⁷⁰

$$q_e = K_F C_e^{1/n} \quad (2)$$

where K_F and n are constants, commonly temperature-dependent. Linearization of the equations can be made favoring the obtainment of the model parameters.

1.4. Solution Blow Spinning

Nanofibers are one-dimensional materials with great potential for application due to their unique physicochemical properties and characteristics. Nanofibers have a high surface area-to-volume ratio and are able to form networks of highly porous mesh with remarkable interconnectivity between their pores. A wide diversity of materials can be used in the preparation of nanofibers through different techniques.⁷²

Solution blow spinning (SBS) has emerged as an interesting technique to produce micro/nanofibers. This technique can produce fibers with diameters ranging from a few tenths of nanometers to several microns, depending on the experimental conditions used.⁷³ In SBS, the setup consists of a source of compressed gas with a pressure regulator, a syringe and a syringe pump to control the injection rate of the solution, a spraying apparatus consisting of two concentric nozzles and a collector. SBS method, differently from the electrospinning method, does not require high voltage equipment or any electrically conductive collector.⁷⁴

In the inner nozzle, a polymer solution is pumped at an appropriate rate and, simultaneously, a high-pressure gas is delivered through the outer nozzle. In the tip of the inner nozzle, a droplet is formed and because of the high pressure and gas velocity from the outer nozzle, it is formed a low-pressure region on the edge of the inner nozzle and the polymer solution is distorted into a conical shape. When a critical air pressure is exceeded, *i.e.* the driving force exerted by the gas overcomes the surface tension force of the solution, the stretching of the cone occurs in the direction

of the gas. The fibers are formed with the evaporation of the solvent between the nozzles and the collector. A wide range of polymer types can be used to obtain the fibers through SBS. The appropriate choice must be made in order to produce a material with the characteristics required for the application to which the material will be intended. Unlike other techniques, in SBS the fibers formed are not attracted to the collector, and can be directed to any target. The fibers are deposited in a one-step process with no further drying, washing or cooling necessary and can be obtained in custom conformal geometries.⁷³⁻⁷⁶

Several parameters can exert influence on the fiber formation and, consequently, on its morphology and characteristics. Solution viscosity, polymer concentration, molecular weight, surface tension and vapor pressure can affect the fiber formation process when using SBS, as well as some other process and system parameters, such as air pressure, working distance, solution flow-rate, nozzle diameter and geometry. Ambient conditions like temperature, humidity and atmospheric pressure can also interfere with the process.^{75,76}

Fibers obtained by SBS have been used in a sort of applications, such as electrodes in fuel cells and supercapacitors, biomedical applications, immobilized enzymes,^{75,76} electrochemical sensors,⁷⁷ sensing units of e-tongues,⁷⁸ substances releasing,⁷⁹ among others. Adsorption is another application in which nanofibers can be used.⁸⁰ The use of nanofibers as adsorbents is interesting due to their high specific surface area per unit mass and high porosity. They can also be properly functionalized, changing their chemical nature and providing materials with different adsorption behaviors.^{81,82} Within this context, poly(methylmethacrylate) (PMMA) nanofibers have interesting properties as adsorbent material and can be obtained by the SBS technique.^{66,83}

2.Goals and Overview

The general goal of this dissertation was to develop and characterize different graphene-based nanomaterials combined with other nanostructured platforms to be employed as sensing units of an electronic tongue in the analysis of components that present a potentially harmful environmental impact and develop a graphene-based nanocomposite with adsorption ability towards a specific dye.

Specific goals

- Synthesis of GO and its further reduction to obtain rGO and the nanocomposites;
- Perform the morphological and physicochemical characterization of the obtained nanomaterials;
- Use of graphene-based materials as sensing units of an e-tongue in the analysis of organophosphorus pesticides;
- Investigation of the performance of a composite membrane obtained using SBS method in the adsorption of the dye methylene blue.

Chapters Overview

Initially, GO was synthesized using an improved eco-friendly Hummers method. The chemical reduction was performed using ascorbic acid, obtaining rGO. The nanocomposites were obtained by reducing the GO in the presence of the chosen polymers and the functionalization with gold nanoparticles occurred in the same reaction medium after the chemical reduction process. The materials were characterized and used to modify gold IDEs to be employed in the electronic tongue. The system was used in the analyses of OP pesticides. Chapter I presents the main results, indicating that the e-tongue was able to respond to the variation of solutions concentration, including real samples and mixtures of OPs pesticides.

Chapter II reports the fabrication of a membrane using SBS technique wrapped with rGO. The composite membrane was used in the adsorption of the methylene blue (MB) dye as a model of wastewater treatment. The adsorption kinetics and isotherm were determined, revealing a great potential of the nanocomposite towards MB adsorption.

General conclusions and future perspectives are presented in the sequence in which the evaluation of the results obtained is made.

3.Chapter I: Electronic tongue based on reduced graphene oxide*

*The content of this chapter is an adaptation of the article entitled: **“Detection of trace levels of organophosphate pesticides using an electronic tongue based on graphene hybrid nanocomposites”** by M. H. M. Facure, L. A. Mercante, L. H. C. Mattoso and D. S. Correa, published in *Talanta*.

Reference: *Talanta*. 2017, 167, 59-66.⁸⁴

3.1. Abstract

Organophosphate (OP) compounds impose significant strains on public health, environmental/food safety and homeland security, once they have been widely used as pesticides and insecticides and also display potential to be employed as chemical warfare agents by terrorists. In this context, the development of sensitive and reliable chemical sensors that would allow in-situ measurements of such contaminants is highly pursued. Here we report on a free-enzyme impedimetric electronic tongue (e-tongue) used in the analysis of organophosphate pesticides comprising four sensing units based on graphene hybrid nanocomposites. The nanocomposites were prepared by reduction of graphene oxide in the presence of conducting polymers (PEDOT:PSS and polypyrrole) and gold nanoparticles (AuNPs), which were deposited by drop casting onto gold interdigitated electrodes. Impedance spectroscopy measurements were collected in triplicate for each sample analyzed, and the electrical resistance data were treated by Principal Component Analysis (PCA), revealing that the system was able to discriminate OPs at nanomolar concentrations. In addition, the electronic tongue system could detect OPs in real samples, where relations between the principal components and the variation of pesticides in a mixture were established, proving to be useful to analyze and monitor mixtures of OP pesticides. The materials employed provided sensing units with high specific surface area and high conductivity, yielding the development of a sensor with suitable stability, good reproducibility, and high sensitivity towards pesticide samples, being able to discriminate concentrations as low as 0.1 nmol L^{-1} . Our results indicate that the e-tongue system can be used as a rapid, simple and low cost alternative in the analyses of OPs pesticide solutions below the concentration range permitted by legislation of some countries.

3.2. Introduction

Organophosphate compounds (OPs) are the largest class of pesticides employed worldwide in the agriculture,^{85–88} which brings serious public concerns regarding the environment, health and food safety.⁸⁹ For instance, such pesticides irreversibly inhibit the enzyme acetylcholinesterase (AChE), which is essential for the normal functioning of the central nervous system in humans and insects, and therefore can inflict respiratory tract injuries, paralysis or even death.⁹⁰ Accordingly, the

development of simple, rapid, and accurate methods to detect OPs residues at low concentrations becomes imperative.^{91,92}

Since the introduction of OPs to the market in the 1970s, many analytical methods have been developed to detect these compounds.⁹³ Mixture of organophosphorus pesticides can be analyzed, detected and quantified by techniques such as gas-chromatography-mass spectrometry,⁹⁴ high-performance liquid chromatography⁹⁵ and liquid chromatography–tandem mass spectrometry,⁹⁶ achieving low limits of detection in the range of ng mL^{-1} . Despite the good sensitivity and the possibility of discriminating different pesticides, these methods require pre-treatment of the sample and sophisticated equipment.⁹⁷

A detection approach capable of discriminating different pesticides in a mixture should provide reliable and robust sensor. At this point, array-based sensing approaches, such as electronic tongues, have emerged as an attractive method.^{97–99} The sensor array makes use of the global selectivity concept. In this type of sensor, although the sensing units may individually present poor selectivity, being considered “nonspecific”, their response together should present cross-sensitivity, namely the ability of the system to respond reproducibly to a wide number of different analytes in solution without specific interaction. Although selectivity is not an essential condition, the system must have stability and high sensitivity.⁵⁴ The use of a sensor array coupled with a chemometric tool, such as a Principal Components Analysis (PCA) employed for data treatment, can substantially improve sensor sensitivity and allow exact identification of the pesticide at trace levels in real samples. In addition, sensor arrays represent a low cost alternative since the system is not composed of sophisticated equipment and does not require a large amount of samples or their pre-treatment.⁵⁷

The unique physicochemical properties of nanomaterials have prompted them as active layers in chemical sensors, in order to enhance the discrimination ability of these sensor arrays.^{56,100,101} In particular, several studies have established graphene as material of choice for the construction of highly sensitive and stable sensors for a variety of analytes.^{13,102–104} In order to further harness the properties and broaden the applications of graphene, some materials have been incorporated to form graphene-based composite nanomaterials.^{105–107} By introducing metal nanoparticles or conductive polymers, for example, the final graphene-based composites will show improved mechanical, electrical or even other properties, resulting in enhanced sensor selectivity and sensitivity.^{34,108} Gold nanoparticles (AuNPs) have been extensively

used in (bio)sensing, including for pesticide detection,¹⁰¹ because of its unique properties and intrinsic electrochemical characteristics.¹⁰⁹ In addition, the electron transfer between conjugated polymers and graphene through a π - π interaction can consequently increase the sensing performance of the hybrid material.¹³

In this work, we propose the use of an impedimetric electronic tongue (e-tongue) to discriminate and analyze mixtures of OPs pesticides in real samples. The sensor array was based on reduced graphene oxide (rGO) and rGO-based nanocomposites, which were characterized by physical chemical techniques, including Fourier transform infrared (FTIR) and UV-vis spectroscopy, Scanning Transmission Electron Microscopy (STEM) and Energy-dispersive Xray (EDX) analysis. By correlating the experimental data using Principal Component Analysis (PCA), the sensor array was capable of detecting OPs pesticides down to nanomolar concentrations in a expedite way.

3.3. Material and methods

3.3.1. Materials

Graphite flakes, sulfuric acid (H_2SO_4), potassium permanganate (KMnO_4), hydrochloric acid (HCl) and hydrogen peroxide (H_2O_2) used in the synthesis of graphene oxide were purchased from Dinamica, Brazil. Ascorbic Acid (AA), polypyrrole (PPy), poly(3,4-ethylenedioxythiophene) poly(styrenesulfonate) (PEDOT:PSS), sodium citrate, hydrogen tetrachloroaurate (III) trihydrate ($\text{HAuCl}_4 \cdot 3\text{H}_2\text{O}$, $\geq 99,9\%$), monopotassium phosphate (KH_2PO_4) and dibasic potassium phosphate (K_2HPO_4) were obtained from Sigma-Aldrich. Malathion and cadusafos pesticides (commercial grade samples) were obtained from FMC (Brazil). The stock solutions of each pesticide were prepared in acetone and stored in amber flasks maintained at 4 °C. All the chemicals were used as received, and double-distilled water was used to prepare all the aqueous solutions. Mineral water was purchased from a local supplier.

3.3.2. Synthesis of nanocomposites

Graphene Oxide (GO) was synthesized according to modified Hummer's method.^{16,17} In a typical procedure, graphite powder (3g) was dissolved in a

concentrated H_2SO_4 (70 mL) solution using an ice bath. KMnO_4 (9g) was slowly added to the mixture in order to keep the temperature of the mixture below 20 °C. The temperature was raised to 40 °C and the system was maintained under vigorous stirring for 30 min. Next, 150 mL of water was added and the resultant mixture solution was maintained at 95 °C. The solution was stirred for 15 min and subsequently 500 mL of water was added followed by the addition of 15 mL of H_2O_2 (30%), leading to a color change of the mixture from brown to yellow. Subsequently, the mixture was filtered and washed with 5% HCl aqueous solution and double-distilled water in order to remove the excessive acid and inorganic salts. The GO was dried overnight at room temperature. Finally, the solid was dispersed in double-distilled water using ultrasonic bath for 30 min. Centrifugation (4000 rpm for 5 min) was used to remove any non-exfoliated material, and the supernatant was stocked for further use.

The synthesis of the nanocomposites used to modify the electrodes was carried out through the chemical reduction of GO using AA as the reducing agent. Reduced graphene oxide (rGO) was synthesized by adding 70 mg of AA in a 50 mL dispersion of GO (0.5 mg mL^{-1}) maintaining the system under reflux for 24 h. PPy-rGO and PEDOT:PSS-rGO nanocomposites were synthesized reducing the GO in the presence of the conducting polymers. In the synthesis, 75 mg of the polymers were added to 50 mL of a GO dispersion (0.5 mg mL^{-1}). After obtaining a homogeneous dispersion, 50 mg of AA were added and the system was kept for 24 h under reflux. The PEDOT:PSS-rGOAuNPs nanocomposite was obtained adding 25 mg of HAuCl_4 and 37 mg of sodium citrate into the solution of PEDOT:PSS-rGO, maintaining the system in reflux for 20 min. The solids were recovered by centrifugation and washed twice with water before use.

3.3.3. Physical chemical characterization

UV–Vis absorption spectroscopy was performed in a Perkin-Elmer Lambda spectrophotometer. Fourier transform infrared (FTIR) spectroscopy was carried out with a Bruker Vertex 70 instrument. The spectra in ATR mode were collected in the range from 2000 cm^{-1} to 400 cm^{-1} with a resolution of 2 cm^{-1} and using 64 scans for each sample. The zeta potential of the solutions was determined using a Zetasizer Nano ZS (Malvern Instruments). A Scanning Transmission Electron Microscope (STEM, FEI Magellan 400 L) was used to evaluate the morphology of the nanocomposites, by which the films were deposited onto a carbon-coated copper grid.

Energy-dispersive X-ray (EDX) analyses were performed using a FEG-SEM (JEOL, JSM 6510) using silicon as substrate.

3.3.4. Interdigitated electrodes (IDEs)

The gold interdigitated electrodes (IDEs) were fabricated by conventional photolithography at the Brazilian Nanotechnology National Laboratory (LNNano). Every IDE is composed by 50 pairs of fingers having length of 4 mm and width and distance between fingers of 10 μm . A digital picture and a scheme of the geometrical features of the IDE employed can be seen in Fig. A1 in Appendix A. IDEs do not require polishing, and analysis can be done using a small sample volume in a wide frequency spectrum. Moreover, the IDEs electrical response can be changed by modifying their shape and geometrical dimensions.¹¹⁰

3.3.5. Impedimetric electronic tongue

Impedance spectroscopy measurements were performed using a Solartron impedance analyzer (1260 A). All sensing experiments were carried out by recording impedance values as a function of frequency from 10 Hz up to 1 MHz using an applied voltage of 50 mV. Once the measurements of an impedimetric e-tongue are performed using a fixed potential, it is not necessary to use a reference electrode usually required for a three-electrode cell employed in electrochemical measurements.⁶⁴

The electronic tongue was composed by four sensing units prepared by drop casting the nanocomposite solutions onto the gold interdigitated electrodes (IDEs), which were used to analyze the pesticides solutions, as illustrated in Fig.3.3.1 (i). The sensing units were characterized by impedance spectroscopy (Fig.3.3.1 (ii)) and the data were treated with the Principal Component Analysis (PCA) method (Fig.3.3.1 (iii)). The following nanocomposite films were used to compose the e-tongue array: rGO, PPy-rGO, PEDOT:PSS-rGO and PEDOT:PSS-rGO-AuNPs.

Prior to the electrode modification, bare IDEs were subjected to impedance measurements in PBS buffer (0.1 mol L⁻¹, pH 7.0) to check the reproducibility of their responses. Such procedure was carried out to ensure that changes in the electrical responses of each modified sensing unit are due to the variation of chemical composition of the nanocomposite films, instead of differences among the IDEs themselves.

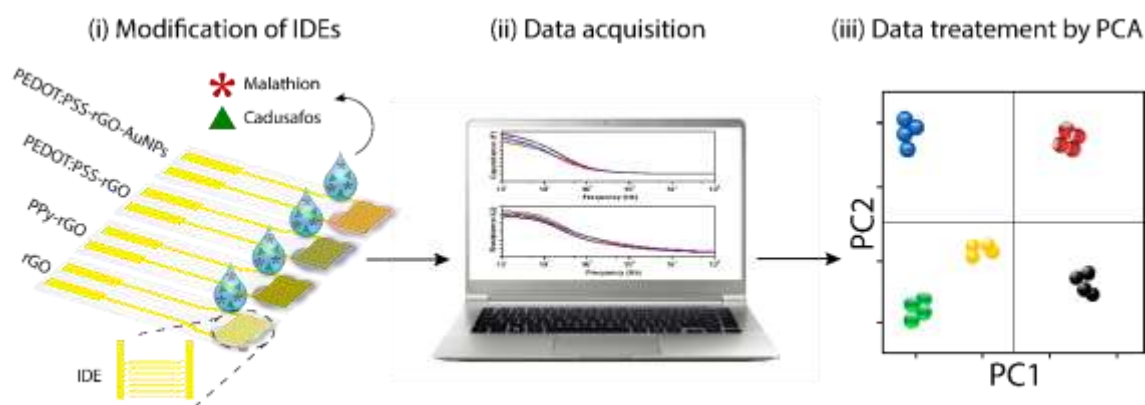


FIGURE 3.3.1: Schematic illustration (i-ii) of the impedimetric e-tongue system based on graphene hybrid nanocomposites for detection of trace levels of OPs pesticides. (iii) PCA was the statistical technique used to treat the electrical resistance data collected by the e-tongue. (Reprinted with permission from Facure *et. al.*⁸⁴)

Three consecutive measurements were performed with each sensing unit immersed in the buffer used as reference, and in the malathion and cadusafos solutions at 0.1, 0.5, 1, and 5 nmol L⁻¹. A solution of each pesticide was first prepared in acetone. These solutions were then diluted with PBS buffer (0.1 mol L⁻¹, pH 7.0) to obtain the stock solutions with a concentration of 30 μmol L⁻¹. The standard pesticides samples used in the measurements were prepared by diluting the stock solution with PBS buffer, while the real samples were prepared by diluting it with tap water. The measurements started with the buffer and then from the lowest (0.1 nmol L⁻¹) to the highest (5 nmol L⁻¹) concentration of pesticide solution. The sensing units were left soaking into the solution 10 min before data acquisition.

3.3.6. Data treatment

The experimental data collected with the electronic tongue were treated with a statistical method known as Principal Component Analysis (PCA), which uses a mathematical algorithm that identifies directions, the principal components (PC) that present the maximum variation of the data. Therefore, a reduction in the dimensionality of the data is achieved while retaining most of the variation in the data set. The first principal component (PC1) represents the direction along which the samples show the largest variation. The second principal component (PC2) is the next component that presents the largest variation, being uncorrelated to the first one. The PCA plot

obtained shows the maximized variance of the samples and allows visualization of the treatment. The PCA plot is used to determine if the samples can be grouped through the evaluation of differences and similarities between them.⁶⁰

3.4. Results and discussion

3.4.1. Nanocomposites characterization

The chemical reduction of GO and the formation of the hybrid nanocomposites were evaluated by UV–vis absorption and FTIR spectroscopies. The UV–vis absorption spectra are presented in Fig. A2 in Appendix A. The spectrum of rGO (i) displays a single absorption band at 271 nm that arises from a redshift of the GO absorption peak, indicating a restoration of the electronic conjugation and the successful reduction of GO.⁵⁰ The peak related to rGO in the nanocomposites is redshifted to 291 nm due to the π – π interaction between the quinoid rings of the conductive polymers and the planar structure of the rGO. In the spectrum of the PPy-rGO nanocomposite (ii) two peaks of the PPy appear at 225 nm and 415 nm, which are assigned to the π – π^* transition.^{45,111} The composites containing PEDOT:PSS show a peak at 225 nm related to the substituted phenyl groups in PSS and another peak at 890 nm ascribed to the polaron state of PEDOT.^{112,113} The spectrum of the nanocomposite with AuNPs (iv) presents a characteristic peak at 545 nm attributed to the surface plasmon resonance of the nanoparticles.¹¹⁴

The FTIR spectra in the Fig. 3.4.1 confirm the successful synthesis of the materials. The FTIR spectrum of rGO (i) presents only one major peak at 1633 cm^{-1} attributed to C=C stretching, suggesting a restoration of unoxidized graphitic domains after the chemical reduction.¹¹⁵ The peaks associated with the oxygen functional groups characteristic of GO do not appear with significant intensity in the spectrum, confirming the high degree of GO reduction achieved using AA as reducing agent. The PPy-rGO nanocomposite spectrum (ii) presents a peak related to the C=C stretching of rGO in 1630 cm^{-1} and the characteristic peaks of PPy appear at 1554, 1449 and 1030 cm^{-1} , which are attributed to asymmetric and symmetric ring stretching vibration and C-H in-plane deformation vibration, respectively. The presence of peaks at 1157 and 928 cm^{-1} indicates the doping state of PPy.⁴⁷ The spectrum of PEDOT:PSS-rGO

(iii), displays a peak of rGO at 1633 cm^{-1} , in addition to the vibrational bands at 1515 and 1295 cm^{-1} related to C=C and C-C stretching vibrations of the quinoid structure of the thiophene ring, respectively. Moreover, the peaks at 932 and 680 cm^{-1} are related to the C-S bonds in the thiophene ring. The S-O bond and S-phenyl bond in PSS are respectively evidenced by the peaks at 1174 and 1080 cm^{-1} .⁴⁸ The same vibrational peaks of rGO and PEDOT:PSS appear in the spectrum of the nanocomposite with gold nanoparticles (iv), as expected.

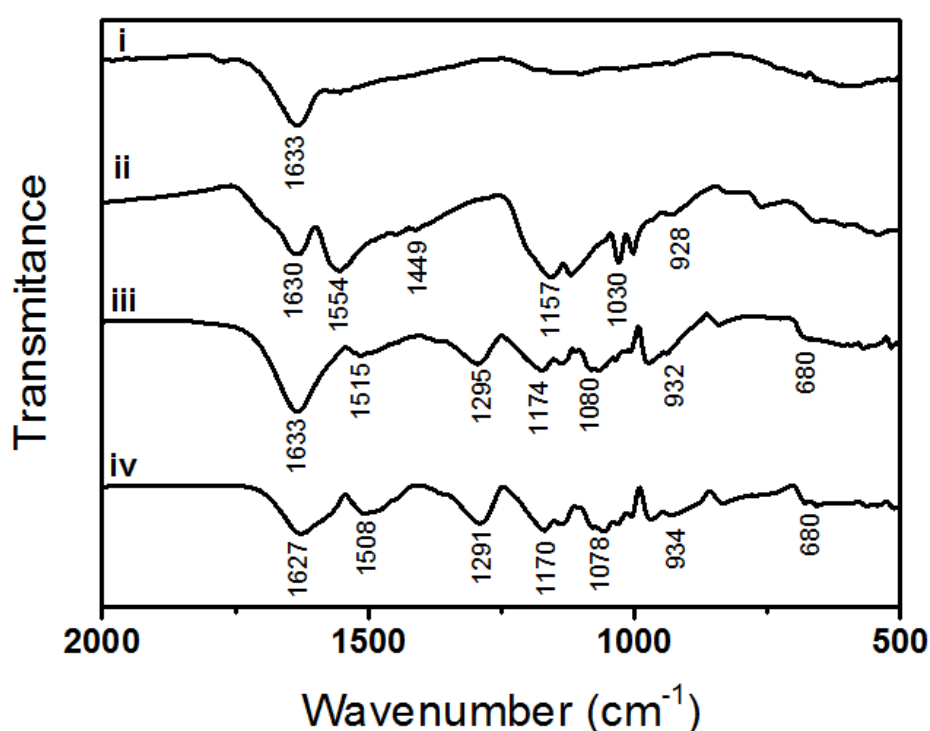


FIGURE 3.4.1: FTIR spectra of rGO (i), PPy-rGO (ii), PEDOT:PSS-rGO (iii) and PEDOT:PSS-rGO-AuNPs (iv). (Reprinted with permission from Facure *et. al.*⁸⁴)

The morphologies of the as-synthesized materials were evaluated by STEM. A typical structure of a crumpled and wrinkled sheet of rGO is observed in Fig. 3.4.2(A). Fig. 3.4.2(B), (C) and (D) show images of the PPy-rGO, PEDOT:PSS-rGO and PEDOT:PSS-rGO-AuNPs hybrid nanocomposite, respectively. It is possible to note that the polymers occurrence provides less aggregation to the rGO sheets, as a result of the strong π - π interaction between the sp^2 -bonded carbon atoms of graphene and the electronic and aromatic structure of PPy and PEDOT:PSS. The polymers tend

to involve and coat the rGO sheets and, as a consequence of the electrostatic repulsive force between them, a higher dispersibility is reached, preventing the restacking of the rGO.^{46,49,116} This is in agreement with the zeta potential experiments: PPy-rGO, PEDOT:PSS-rGO and PEDOT:PSS-rGO-AuNPs dispersions yielded values of -42, -40 and -51 mV, respectively, while the dispersion of rGO presented a value of -22 mV.

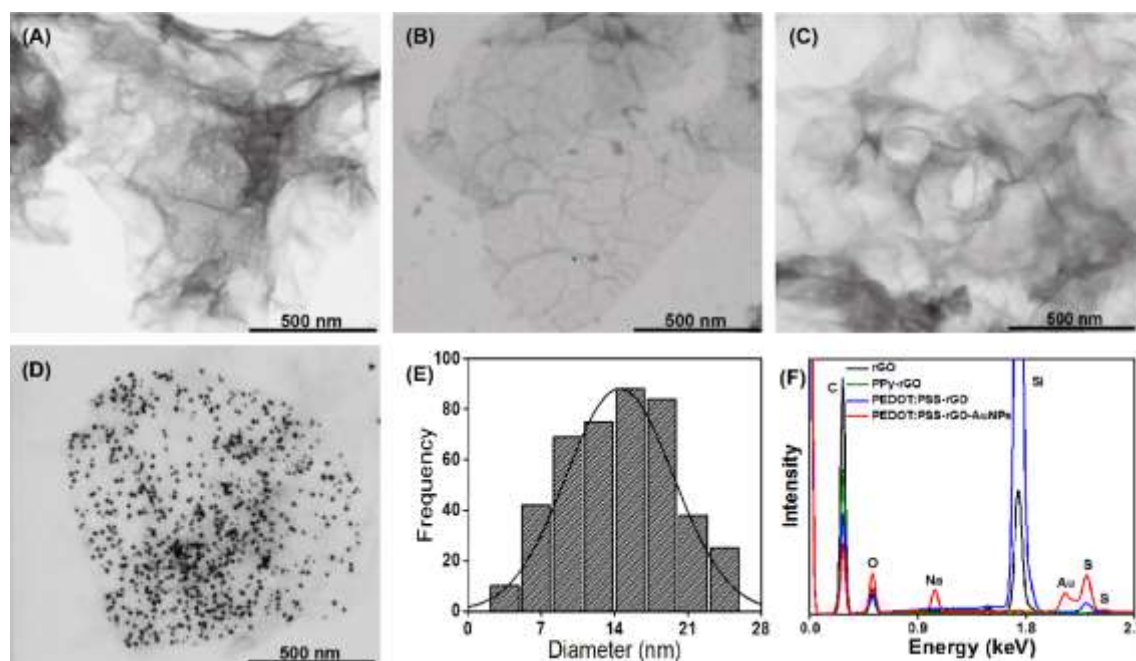


FIGURE 3.4.2: STEM images of (A) rGO, (B) PPy-rGO, (C), PEDOT:PSS-rGO, (D) PEDOT:PSS-rGO-AuNPs, (E) histogram of size distribution of gold nanoparticles and (F) EDX spectra of rGO (black), PPy-rGO (green), PEDOT:PSS-rGO (blue) and PEDOT:PSS-rGO-AuNPs (red). (Reprinted with permission from Facure *et. al.*⁸⁴)

The Fig. 3.4.2(D) shows that the AuNPs are deposited only onto the rGO graphene sheets. The nucleation and the growth of the nanoparticles occur in the reactive sites provided by the oxygen groups remaining in the surface of the rGO that could not be removed during the chemical reduction.¹¹⁷ The average size of the AuNPs was found to be 14.5 nm, and the histogram of the nanoparticles size distribution is presented in the Fig. 3.4.2(E). The EDX analysis showed in Fig. 3.4.2(F) reveals peaks related to C and O elements in all materials and the presence of S element in the nanocomposites containing PEDOT:PSS and Au element in the spectrum of the PEDOT:PSS-rGO-AuNPs nanocomposite, indicating that the nanocomposites were synthesized successfully. There is a peak of low intensity related to N element in the

spectrum of the PPy-rGO nanocomposite at around 0.39 keV, indicating the presence of the polymer in the material. The presence of N element is confirmed in the EDX mapping images presented in Fig. A3 in the Appendix A. The peaks related to Si element appear because of the substrate employed and due to the thickness of the films evaluated. The presence of Na element arises from residual sodium citrate used in the reduction of Au nanoparticles.

3.4.2. Impedimetric electronic tongue experiments

Before using the IDEs modified by rGO and the rGO-based nanocomposites in the impedimetric e-tongue system for the detection of the pesticides, measurements in PBS buffer (0.1 mol L^{-1} , pH 7.0) were performed. Such experiments aimed at determining the optimized frequency in the impedance spectroscopy measurements for yielding the best samples discrimination ability. Fig. 3.4.3 shows the electrical resistance curves of each sensing unit.

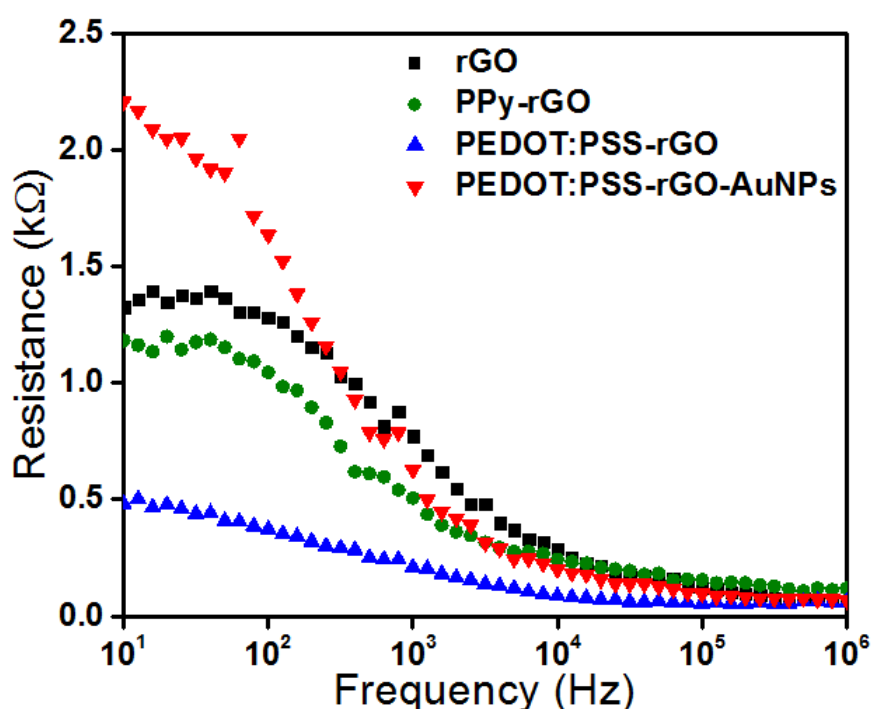


FIGURE 3.4.3: Resistance versus frequency data for each sensing unit in PBS buffer solution (0.1 mol L^{-1} , pH 7.0). (Reprinted with permission from Facure *et. al.*⁸⁴)

The responses in the lower frequency region (< 100 Hz) are governed by the double-layer effect, while at higher frequencies (> 100 kHz) the impedance is governed by the geometric capacitance. The films coating the electrodes governs the responses at the intermediate frequency region, from 100 Hz to 100 kHz.⁵⁸ Based on Fig. 3.4.3, all the experimental data in this work will be correlated through PCA by grouping the information from electrical resistance values at 100 Hz, a frequency at which the effects from the materials coating the electrodes are more evident. In addition, the deposition of the conducting films onto the gold IDE's caused an expected substantial decrease in electrical resistance (almost 92%), indicating that the films altered deeply the electrical responses of bare electrodes.

3.4.2.1. Different pesticides and concentrations

To fully explore the different sensitivities of the rGO based nanomaterials, an electronic tongue based on an array of 4 IDEs modified by rGO, PPy-rGO, PEDOT:PSS-rGO and PEDOT:PSS-rGOAuNPs was first used to perform discrimination of OPs pesticides in PBS buffer solution (0.1 mol L^{-1} , pH 7.0). In a first investigation, PCA (Fig. 3.4.4) was employed to interpret the response of the e-tongue collected at 100 Hz to individual malathion (A) and cadusafos (B) solutions in nanomolar range. In both PCA plots, all the samples are clearly discriminated, presenting no superposition between distinct groups (buffer, 0.1, 0.5, 1.0 and 5.0 nmol L^{-1}) and a proximity of triplicate points of the same sample can be seen, indicating high reproducibility of the measures. The high PC1 values obtained (PC1 accounts for 92.77% and 97.01% of the data variance for the malathion and cadusafos, respectively), indicate a good correlation of the data.^{55,56,118} It is worth mentioning that there is a correlation between sample concentration and PC1 axis (as the concentration of the pesticides solutions increases, the samples tend to locate more to the right side of PC1) clearly indicating that the array was capable of discriminating the solutions in nanomolar concentrations. Such concentration range, for instance, is below the acceptable concentration for the use of malathion by Brazilian legislation.¹¹⁹

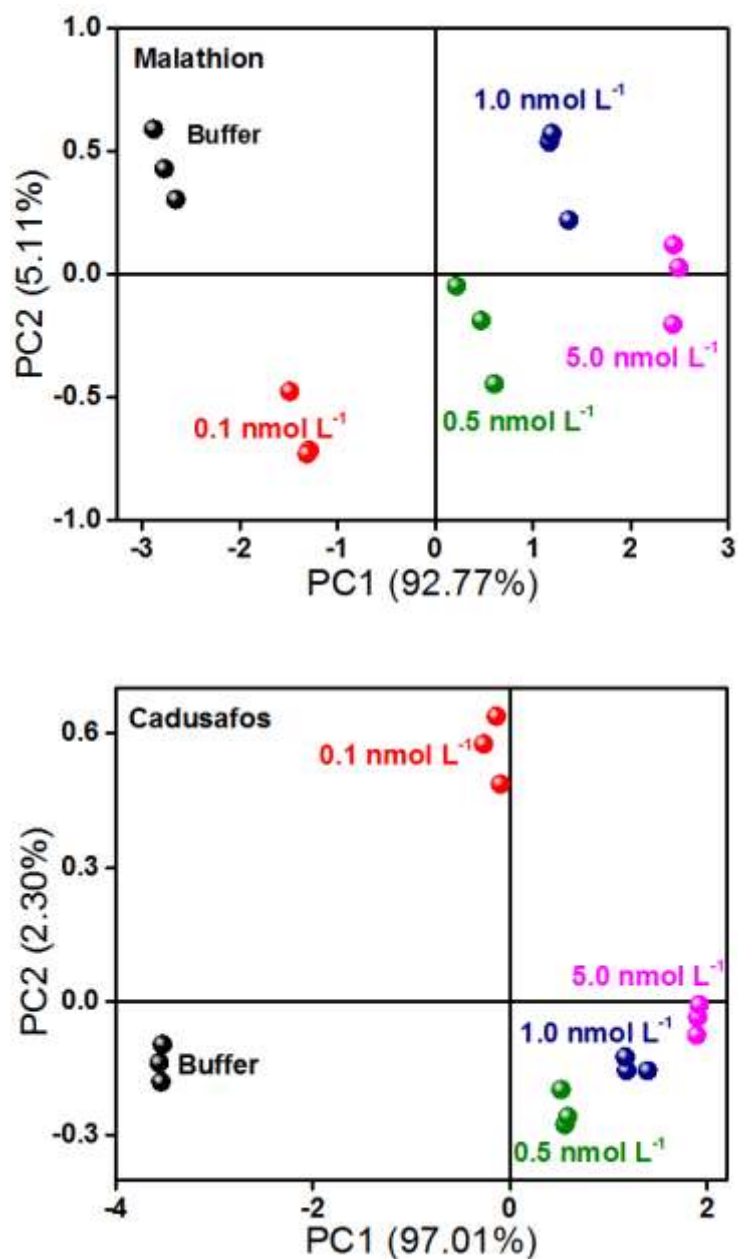


FIGURE 3.4.4: PCA plots for the electrical resistance responses (experimental data collected with the electronic tongue) at 100 Hz for the analysis of malathion (A) and cadusafos (B) diluted solutions. (Reprinted with permission from Facure *et. al.*⁸⁴)

When these data are plotted in a single PCA (Fig. 4.3.5), the separation of the solutions by concentration is also observed and the right hand trend with the increase of the solutions concentration is maintained. The PCA graph also shows that the e-tongue is able to clearly discriminate the samples of different pesticides, and again a high PC1 value is obtained (88.98%).

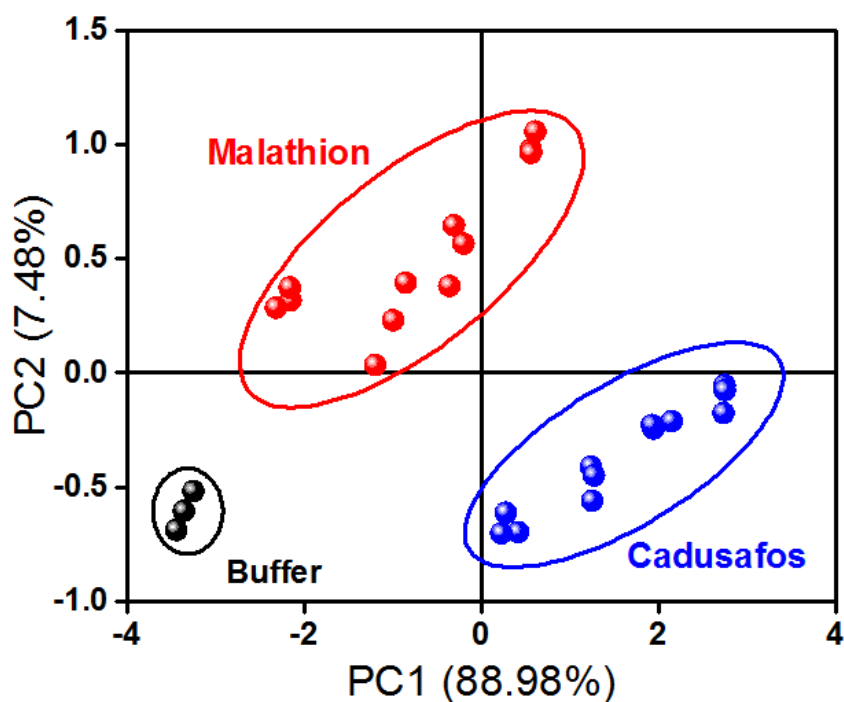


FIGURE 3.4.5: PCA plot for the electrical resistance responses (experimental data collected with the electronic tongue) at 100 Hz for the analysis of malathion and cadusafos solutions. (Reprinted with permission from Facure *et. al.*⁸⁴)

3.4.2.2. Mixture of pesticides

In order to simulate a real sample analysis, we prepared and analyzed PBS solutions contaminated with different amounts of both pesticides. Sixteen solutions were prepared making a combination of the concentrations used previously. The array was again able to discriminate all the solutions, yielding a PCA without any superposition of the distinct groups of samples, while a good proximity of the samples having the same pesticide concentrations could be observed. When the concentration of one pesticide is fixed at 1 nmol L⁻¹, the average value of the PC1 varies linearly with the concentration of the other pesticide, as displayed in Fig. 3.4.6. The linear regression curves obtained when the concentration of malathion (Fig. 3.4.6A) and cadusafos (Fig. 3.4.6B) in the solutions was varied yielded R² values of 0,997 and 0,987, respectively.

These results represent an interesting alternative for the analysis and monitoring of organophosphate pesticides mixtures, since biosensors using AChE have no selectivity for different OP pesticides, once the responses are due the inhibition of the enzyme activity, responding to the global amount of OP pesticides

present in the mixture.⁸⁹ Our e-tongue proved to be useful to analyze the variation of the concentration of OP pesticides in a mixture at a nanomolar range.

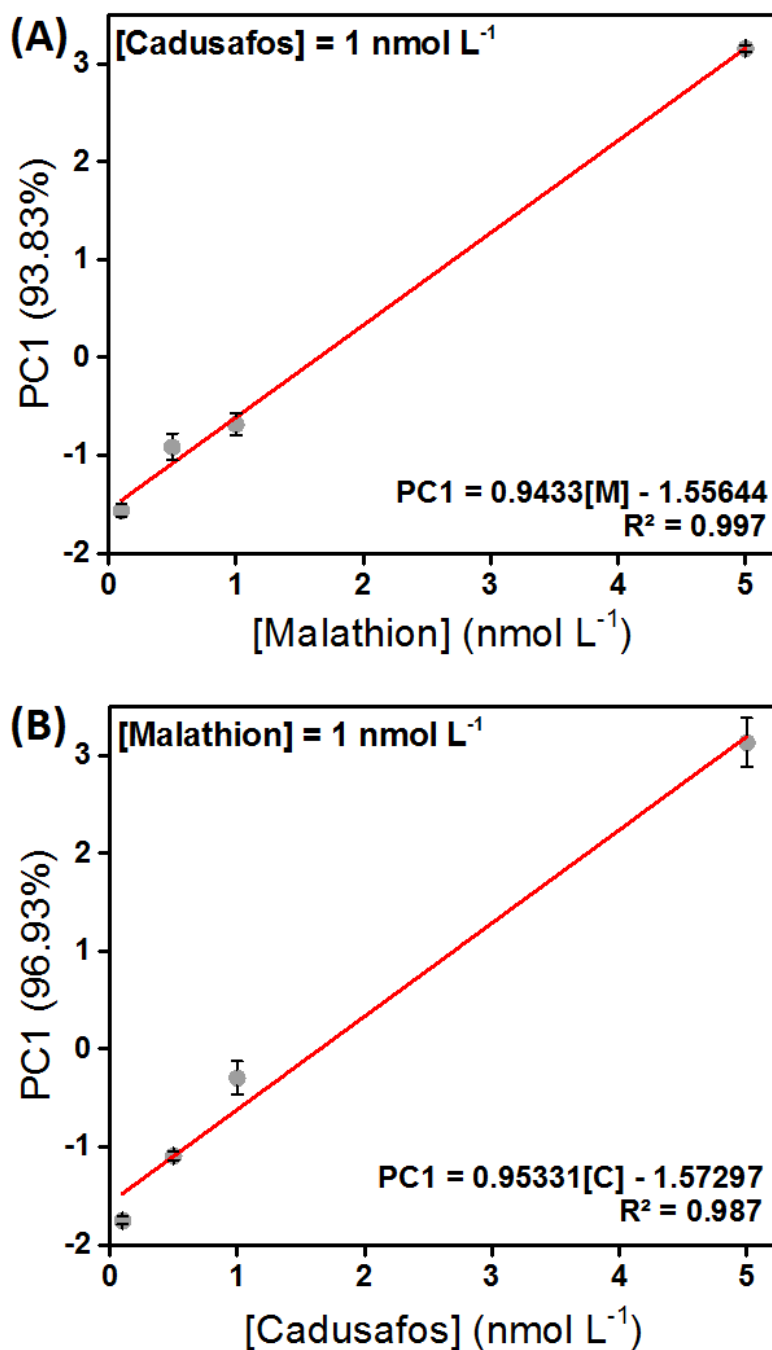


FIGURE 3.4.6: PC1 average values versus the concentration of malathion (A) and cadusafos (B) and the respective linear regression. (Reprinted with permission from Facure *et. al.*⁸⁴)

3.4.2.3. Real samples

Although PBS buffer was very appropriate to carry out the previous studies, the tightly controlled composition cannot be strictly compared to real samples analysis. Based on this aspect, malathion and cadusafos solutions were also prepared using tap water at 0.1, 0.5 and 1.0 nmol L⁻¹ and further evaluated with our e-tongue system. The PCA displayed in Fig. 3.4.7 was obtained using the electrical resistance responses at 100 Hz of the real samples, the samples prepared in buffer solution and mineral water, tap water and PBS buffer. The PCA shows that the e-tongue is very effective in differentiating the real samples from the samples prepared in buffer solution and from tap water, again yielding a very clear separation of different groups. From the PCA plot, one observes no superposition of the distinct samples, where PC1+PC2 accounts for 99.50% of the total variance collected by the sensor array. The concentrations of real samples of both pesticides presented a correlation with the values of PC1 and PC2. When the concentration of the pesticides in the real samples increases, the value of the PC1 also increases for cadusafos samples and decreases for malathion samples. The PC2 value, in turn, decreases with the increase of the concentration of cadusafos and increases for malathion. Additionally, the concentrations of the samples prepared in PBS buffer solution present a direct relation mainly with the PC2 value.

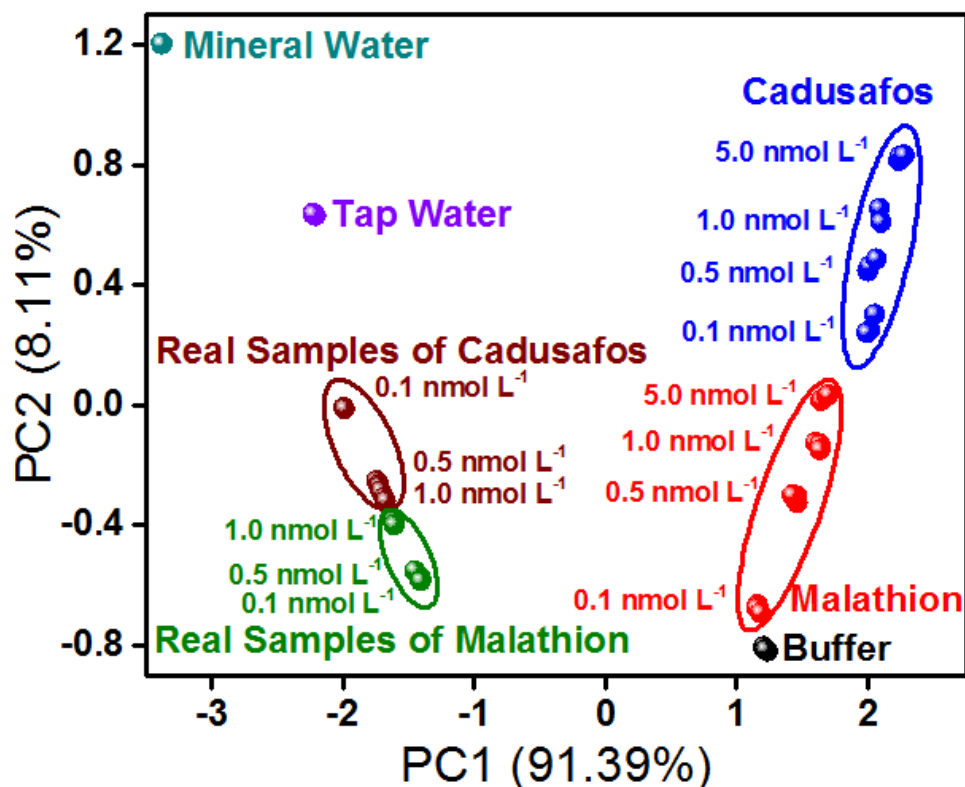


FIGURE 3.4.7: PCA plot for the electrical resistance responses (experimental data collected with the electronic tongue) at 100 Hz for the analysis of malathion and cadusafos solutions prepared with PBS buffer solution and tap water (real samples). (Reprinted with permission from Facure *et. al.*⁸⁴)

The choice of graphene as the base material of the e-tongue sensing units proved to be quite suitable for discriminating the pesticides samples. Its interesting characteristics such as high specific surface area, high conductivity, good chemical stability and low electrical noise, increase the signal-to-noise ratio and provide better sensing responses for the electronic tongue. Moreover, the use of rGO yields a platform with high conductivity presenting residual oxygen-containing groups, which work as active sites providing high sensitivity and allowing the detection of the pesticides at nanomolar concentrations.^{102,120,121} The combination of conducting polymers and gold nanoparticles with rGO makes possible to achieve sensing units with dissimilar architectures, which display different surface charge and functional groups, while maintaining high specific surface area and high conductivity.^{122–124} By comparing the proposed platform with other electrochemical sensors designed for the detection of malathion^{125,126} or other OPs pesticides making use^{127,128} or not of AChE,⁸⁹ and with previous works using e-tongue,^{118,129} it is possible to conclude that the sensor

developed here presents high sensitivity once it could detect malathion and cadusafos at concentrations as low as 0.1 nmol L^{-1} .

3.5.Conclusion

Novel graphene-based nanocomposites were synthesized and successfully used as sensing units of a free-enzyme electronic tongue aiming at detecting trace levels of organophosphates pesticides. The rGO associated with conductive polymers and gold nanoparticles granted good stability, high reproducibility and high sensitivity to the developed e-tongue. Making use of the PCA analysis, the e-tongue was able to classify solutions of different pesticides at distinct nanomolar concentrations, and discriminate real samples from the samples prepared in buffer solutions, presenting a correlation with the concentration and the value of the PC component. The sensor array was also capable of discriminating mixtures containing two organophosphate pesticides, presenting a linear correlation of the PC1 value with the variation of one of the pesticides in the solution, representing a breakthrough for sensing and analysis of organophosphate pesticides mixtures.

4. Chapter II: PMMA nanofibers modified with reduced graphene oxide as adsorbent*

*The content of this chapter is an adaptation of the article entitled: **“Solution blow spun PMMA nanofibers wrapped with reduced graphene oxide as an efficient dye adsorbent”** by L. A. Mercante, M. H. M. Facure, D. A. Locilento, R. C. Sanfelice, F. L. Migliorini, L. H. C. Mattoso and D. S. Correa, published in *New Journal of Chemistry*.

Reference: *New J. Chem.* 2017, 41, 9087-9094.¹³⁰

4.1. Abstract

Nanotechnology has provided innovative solutions to guarantee sustainable energy and maintain a clean environment for the future. In this regard, 1D nanostructured materials, such as nanofibers, are very attractive, especially for the development of economic and environmentally friendly approaches for wastewater treatment. Recently, Solution Blow Spinning (SBS) has appeared as a powerful fiber forming technique with several advantages compared to the traditional electrospinning method. Herein, we present the fabrication of composite membranes using solution blow spun poly(methylmethacrylate) nanofibers wrapped with reduced graphene oxide (PMMA-rGO) to adsorb methylene blue (MB), which is a typical dye used in the printing and dyeing industry. The dye adsorption kinetics and isotherm follow the pseudo-second-order and the Langmuir models, respectively. The π - π stacking interactions were considered to be the major driving force for the spontaneous adsorption of MB and the maximum adsorption capacity was 698.51 mg g⁻¹ according to Langmuir fitting. The developed nanocomposite shows great potential for decolorizing dyeing wastewater aimed at industrial and environmental remediation applications.

4.2. Introduction

Water contamination has nowadays become a global problem due to the intensification of industrial and agricultural activities. As a class of water pollutants, organic dyes used in varied industrial processes can be found widespread in the environment as long-life residual products.^{37,131} In addition to their unwanted colors, some of these dyes may degrade to produce carcinogens and toxic products.¹³² In this context, attempts to develop novel materials and nanofiber membranes with high surface area and porosity at a low cost for efficient remediation of dyes are highly keen. Also, the possibility of incorporating a variety of functionalities to the nanofibers, prior or after the spinning process, enables the tuning of the sorbent properties for specific pollutants.¹³³

Graphene-based composite nanomaterials have shown excellent performance for environmental applications as adsorbent materials.^{37,134} For instance, their large surface area, delocalized π network and easy scalable production have been exploited in the adsorption of different types of contaminants.^{35,135-137} Their

nanosized structures also endow them some advantages such as rapid equilibrium rates, high adsorption capacity and effectiveness over a broad pH range.¹³⁸ Adsorption capacity depends on the surface properties of the adsorbent, in which the sites available to interact with the pollutants and the homogeneous dispersity in aqueous media are important factors in the case of graphene-based materials.¹³⁶ Although the diverse oxygen functionalities of graphene oxide (GO) provide the material with hydrophilicity, at the same time they also provide a weak π electron structure that results in a poor affinity for aromatic pollutants.¹³⁶ Reduction of GO nanosheets allows the recovery of its adsorption capabilities by giving back the π -delocalized electron system. However, reduced graphene oxide (rGO) tends to aggregate due to strong intermolecular (specially, π - π and van der Waals) interactions between the layers, thus reducing the number of potential adsorption sites of graphene. In order to overcome such undesirable aggregation, loading rGO onto low-cost substrates has proven to be a promising alternative.¹³⁹ In this scenario, inexpensive spun nanofibers appear as an ideal framework material that can be used to support rGO nanosheets, preventing their agglomeration.

More recently, the solution blow spinning (SBS) technique has been developed as a promising micro/nanofiber mat fabrication technology.^{73-76,140} This method uses high speed gas flow as the driving force to blow polymer solution streams to ultrathin jets and nanofibers.⁷⁴ The process has received considerable attention due to its easy handling and high productivity for mass production of nanofibers.¹⁴¹ In comparison to electrospinning, one of the most widely employed fiber fabrication technique,¹⁴² SBS has fewer process requirements and variables, does not require a high voltage source and a metallic target and has a deposition rate that is approximately 10 times faster than conventional electrospinning.⁷⁴

Herein, we present an efficient dye decontamination strategy based on the development of free-standing poly(methylmethacrylate)-reduced graphene oxide (PMMA-rGO) composite nanofiber membranes used to adsorb the dye methylene blue (MB). The PMMA-rGO composite was prepared by solution blow spinning PMMA followed by a three-step process: (i) plasma treatment of the PMMA surface, (ii) GO adsorption and (iii) GO reduction. The produced composite nanofibers were characterized by scanning electron microscopy (SEM), BET surface area analysis, Fourier transform infrared (FTIR) spectroscopy and contact angle measurements. The reduced graphene oxide coated-PMMA nanofibers demonstrated superior adsorption

capabilities as compared to their homologous PMMA and PMMA-GO counterparts. The fact that the graphene adsorption sites are fully expressed on the surface of a low-cost nanofiber membrane-based substrate offers the possibility of an efficient pollutant removal process, which opens up new possibilities for environmental remediation.

4.3. Experimental

4.3.1. Materials

Poly(methylmethacrylate) (PMMA, $M_w = 350\,000$), methylene blue (MB) and ascorbic acid were purchased from Sigma- Aldrich. Acetone and chloroform were purchased from Synth Chemical (São Paulo, Brazil). Graphite flakes, potassium permanganate ($KMnO_4$), sulfuric acid (H_2SO_4), hydrochloric acid (HCl) and hydrogen peroxide (H_2O_2) were obtained from Dinamica, Brazil. All the chemicals were used as received.

4.3.2. Preparation of PMMA spun nanofibers by SBS

PMMA was dissolved in chloroform : acetone at 3 : 1 (v/v) under vigorous stirring for 2 h at room temperature to prepare a 10% (w/v) polymer solution.

The SBS apparatus⁷⁴ was composed of a polymer injection pump, a collector consisting of a spinning cylinder positioned horizontally, a source of compressed air and a concentric nozzle system, as illustrated in Fig. 4.3.1. This system is composed by an inner nozzle (0.5 mm in diameter), through which the polymer solution is injected at a rate of 7.2 mL h^{-1} , and an outer nozzle, through which compressed air is delivered at a constant pressure of 300 kPa. The inner nozzle was positioned so that it protruded 2 mm from the outer nozzle. SBS nanofibers were deposited directly onto the collector spinning at 300 rpm, which was positioned at a fixed working distance of 12 cm from the nozzle system.

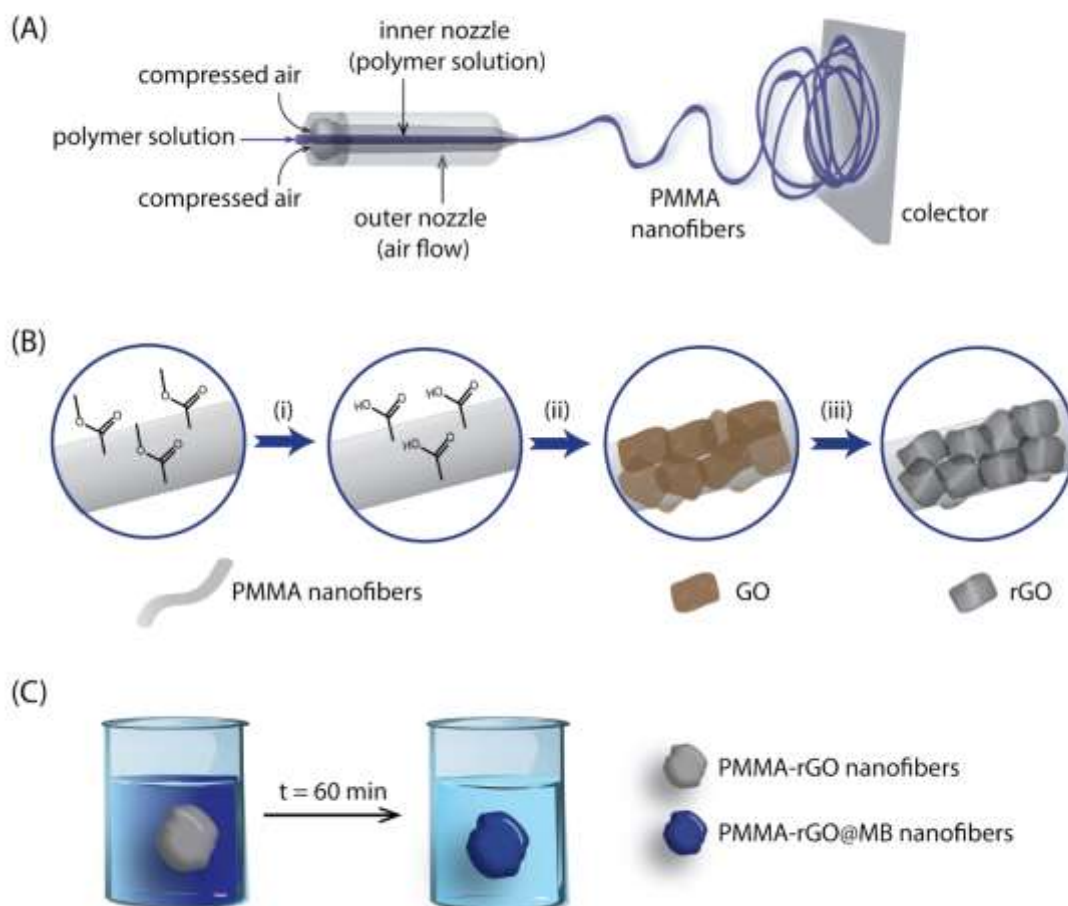


FIGURE 4.3.1: Sketch of the steps involved in the preparation of PMMA-rGO composite nanofibers: (A) solution blow spinning PMMA nanofibers and (B) surface modification: (i) plasma treatment, (ii) GO adsorption and (iii) GO reduction. (C) Scheme of the decontamination process of MB-containing water using the developed composite nanofibers. (Reprinted with permission from Mercante *et. al.*¹³⁰)

4.3.3.Synthesis of GO

Graphene oxide (GO) was synthesized from graphite flakes by employing an eco-friendly modified Hummers method.¹⁷ In brief, graphite powder (3 g) was added to an ice bath containing concentrated H₂SO₄ (70 mL) solution. KMnO₄ (9 g) was slowly added to the solution, while maintaining the temperature below 20 °C. After complete dissolution, the system was maintained under vigorous stirring at 40 °C in an oil bath for 30 minutes. Subsequently, 150 mL of water was added, increasing the temperature to about 95 °C, and the mixture was stirred for 15 minutes. After another addition of 500 mL of water, 15 mL of H₂O₂ (30%) was added to the solution, changing its color

from brown to yellow. The mixture was filtered and washed with diluted HCl (1 : 10) and distilled water several times to remove any excessive acid and inorganic salts. The resulting GO was dried overnight at room temperature.

4.3.4. Surface functionalization of PMMA nanofiber mats with rGO

Before the functionalization, the as-prepared PMMA spun nanofiber membranes were subjected to plasma treatment (SPI Plasma Prep II system) for different etching times (15, 30 and 60 s) and the time period of 30 s was chosen for subsequent studies. Then, the nanofiber membranes were coated with GO by means of immersion in an aqueous suspension of GO (0.5 mg mL⁻¹). Different adsorption times for GO were also tested (30 min, 1 and 2 h) and the time period of 1 h was chosen for further studies (see Fig. B1 in Appendix B). The resultant PMMA-GO composite was washed three times and dried under ambient conditions before immersion in a 0.3 mg mL⁻¹ ascorbic acid solution for the reduction of the GO-wrapped nanofibers. The mixture was allowed to stir for 48 h, washed 3 times with distilled water and dried overnight at room temperature.

4.3.5. Dye adsorption experiments

For the adsorption experiments, MB was chosen as a model dye. The dye adsorption experiment was performed in a 100 mL beaker under ambient conditions. The beaker was filled with a MB solution (100 mg L⁻¹, 50 mL). Then, 15 mg of PMMA-rGO nanofiber mats were added to the beaker. At each time interval, 1.5 mL of the solution was collected. The sample was then diluted to 3 mL with water to analyze MB adsorption efficiency by using a Lambda-25 UV-vis spectrometer (Perkin Elmer). The dye removal efficiency ($R_t, \%$) and adsorption amount ($q_t, \text{mg g}^{-1}$) at time t were calculated using eqn (3) and (4), respectively:

$$R_t = \frac{(C_0 - C_t)}{C_0} \times 100 \quad (3)$$

$$q_t = \frac{(C_0 - C_t)V}{m} \quad (4)$$

where C_0 is the initial concentration (mg L⁻¹), C_t is the concentration at time t (mg L⁻¹), V (L) is the volume of MB solution and m is mass of the fiber membrane (g). For the

desorption experiment, the PMMA-rGO@MB nanofibers were washed thoroughly with deionized water. Then the fibers were put in ethanol solution containing 2% (v/v) NaOH. After desorption equilibrium, the fibers were washed several times with deionized water and were reused in the next cycle of the adsorption experiment.

4.3.6. Characterization

The morphology and size of the samples were evaluated using a Scanning Electron Microscope (JEOL JSM-6510). The average fiber diameter was estimated using the Scanning Electron Microscopy (SEM) images with the aid of an image analysis software program (Image J, National Institutes of Health, USA).

Contact angles of water drops on the surface of spun fibers (nonwoven mats) were measured using a contact angle measuring system (CAM 101 model KSV Instruments) equipped with a CCD camera (KGV-5000). For each measurement, a 5 μL droplet was pipetted onto the mat surface, and the images of the droplet were automatically taken as a function of time. From these images, contact angle values were calculated using dedicated software (KSV CAM 2008).

The surface area of PMMA nanofibers was calculated according to the Brunauer–Emmett–Teller (BET) method, using N_2 adsorption data obtained in a ASAP-2020 system (Micromeritics).

Fourier transform infrared (FTIR) spectra of samples were recorded using a Bruker Vertex 70 equipment. The spectra were collected in ATR mode from 2000 cm^{-1} to 600 cm^{-1} . A total of 64 scans were collected at a resolution of 2 cm^{-1} .

4.4. Results and discussion

4.4.1. Characterization of PMMA-rGO composite fiber membranes

A facile spinning-based strategy was developed to fabricate composite nanofiber membranes for dye adsorption. The preparation process of the PMMA-rGO composite spun nanofibers is illustrated in Fig. 4.3.1, including solution blow spinning PMMA nanofibers, plasma treatment of the PMMA surface, GO adsorption and GO reduction.

Scanning electron microscopy (SEM) was applied to investigate the structural morphology of PMMA and PMMA-GO nanofibers (Fig. 4.4.1). Fig. 4.4.1a

shows PMMA nanofibers randomly orientated with a diameter of 642 ± 169 nm. Furthermore, BET analysis for the PMMA spun membranes revealed that the surface area of the fibers was $16 \text{ m}^2 \text{ g}^{-1}$. This value is similar or even higher when compared to other polymeric nanofibers.^{143,144}

Plasma treatment was a key step to the successful chemical modification of PMMA fibers with GO, as illustrated in Fig. 4.4.1b and c. In Fig. 4.4.1b, it is clearly seen that the GO sheets only cover part of the nanofiber surface, while a large portion has no GO. However, the GO sheets uniformly covered the entire surface of the nanofibers after the plasma treatment was applied for 30 s (Fig. 4.4.1c). The characteristic veil-like structure of graphene materials can be seen covering the whole surface area of the nanofibers in Fig. 4.4.1d (magnified image of panel c).

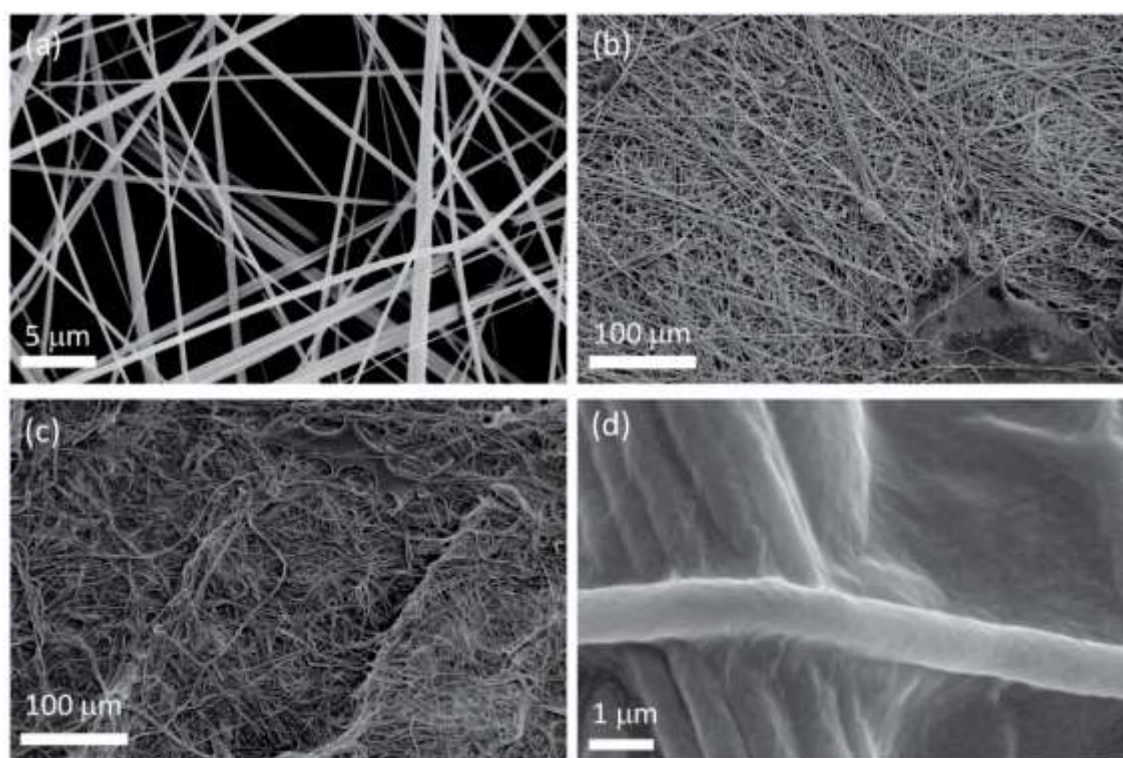


FIGURE 4.4.1: SEM images of (a) PMMA nanofibers, (b) PMMA-GO nanofibers without and (c) with plasma treatment. (d) Magnified image of panel (c). (Reprinted with permission from Mercante *et. al.*¹³⁰)

With the process of plasma etching, oxygen-containing functional groups can be generated on the surface of the PMMA nanofibers, as evidenced by the variation of the water contact angle for the fiber membranes (Fig. 4.4.2). The untreated

PMMA surface has a large contact angle value of about 114° . With the plasma treatment, the contact angle of the PMMA nanofiber mats decreased, which reveals a modification in the surface chemistry. The hydrophobic surface of the PMMA fiber mats becomes quite hydrophilic upon plasma etching for 30 s, due to plasma-induced oxidation of the surface methyl groups, causing the surface of the film to become more hydrophilic.¹⁴⁵ Together with the SEM images (Fig. 4.4.1), we can conclude that plasma etching for 30 s produced enough hydrophilic functional groups on the surface of the PMMA nanofibers leading to a uniform decoration of the GO. The interaction between the plasma treated PMMA nanofibers and GO is mainly due to the presence of hydrogen bonds between the hydroxyl groups of GO and the carboxyl groups of PMMA (after plasma treatment).¹⁴⁶

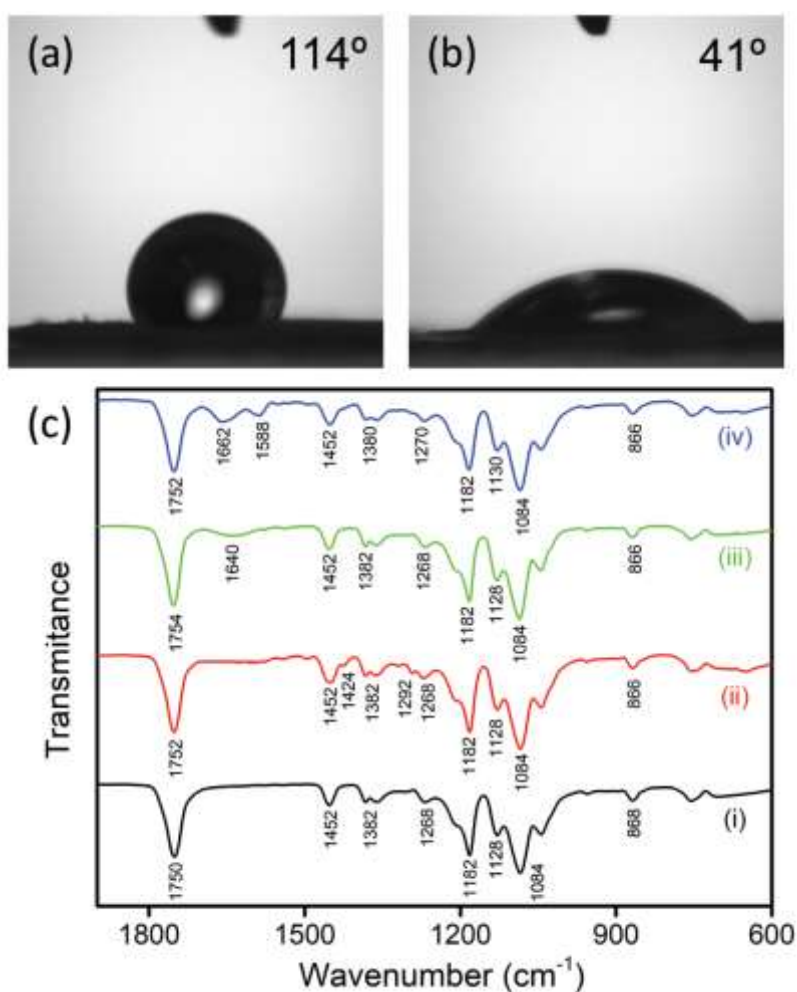


FIGURE 4.4.2: Photographs of a water droplet on PMMA fibers (a) before and (b) after plasma treatment. (c) FTIR spectra of pure PMMA (i), PMMA-GO (ii), PMMA-rGO (iii) and PMMA-rGO@MB (iv) nanofibers. (Reprinted with permission from Mercante *et al.*¹³⁰)

To further evaluate how the changes in surface properties affected the adsorption capability of the composite material, the chemical reduction of GO-coated nanofibers was performed with an environmentally friendly ascorbic acid-based method.¹⁷ Chemical reduction of GO results in a stable rGO layer which significantly altered the surface chemistry of graphene oxide (including loss/conversion of surface O-functional groups and partial recovery of the π electron structure), and consequently, had marked effects on the adsorption affinities of the carbon nanomaterials.¹⁴⁷

To better understand the chemical composition of the nanofiber coating with GO or rGO, FTIR analyses were done (Fig. 4.4.2c). As noted, all the spectra show the characteristic bands of PMMA at 1750 (C=O), 1452 (C-H), 1382 (O-CH₃), 1268 (C-C-O), 1128 (C-O-C) and 868 (C-O-C) cm⁻¹.^{83,148} The spectrum of PMMA-GO, in addition to the characteristics of PMMA, displays the vibrational bands at 1424 and 1292 cm⁻¹ related to epoxy C-O and alkoxy C-O stretching vibrations of GO, respectively. After the reduction with ascorbic acid, these peaks disappeared and a new vibrational band, attributed to the C=C stretching, appears at 1640 cm⁻¹, suggesting a restoration of the carbon basal plane in rGO.⁸⁴

Each modification step was also monitored and confirmed by digital photographs, as illustrated in Fig. 4.4.3a. After modifying the white PMMA nanofiber membrane by immersing it in the suspension of GO, the material surface became brown. After GO reduction with ascorbic acid, the color of the nanofibers changed to black, thereby confirming the formation of PMMA-rGO nanocomposites.

4.4.2. Dye adsorption studies

MB, an aromatic heterocyclic cationic dye, was selected as a model contaminant to examine the adsorption capability of the rGO-modified nanofibers. The static adsorption studies were carried out by adding 15 mg of the nanofiber membrane to a 50 mL solution containing an initial MB concentration of 100 mg L⁻¹. After exposure of the nanofiber mat to the MB solution, the blue color of MB gradually faded with time and the characteristic absorption peak of MB solution at 665 nm gradually decreased (Fig. 4.4.3b). When the exposure time was extended to 60 min, the peak at 665 nm tended to be flat, indicating that most of the MB was adsorbed onto the fiber surface. In addition, the nanofiber mat became blue (Fig. 4.4.3a) after immersion in the MB aqueous solution, further confirming the adsorption of MB molecules onto the membrane. After the adsorption equilibrium was achieved, the final adsorption capacity

of the composite nanofibers for MB was determined to be 230.7 mg g^{-1} . The adsorption capacity of MB was found to be 163.3 mg g^{-1} for the second cycle, which represents 71% of the capacity determined in the first adsorption process, demonstrating reasonable stability and reutilization of the composite material.

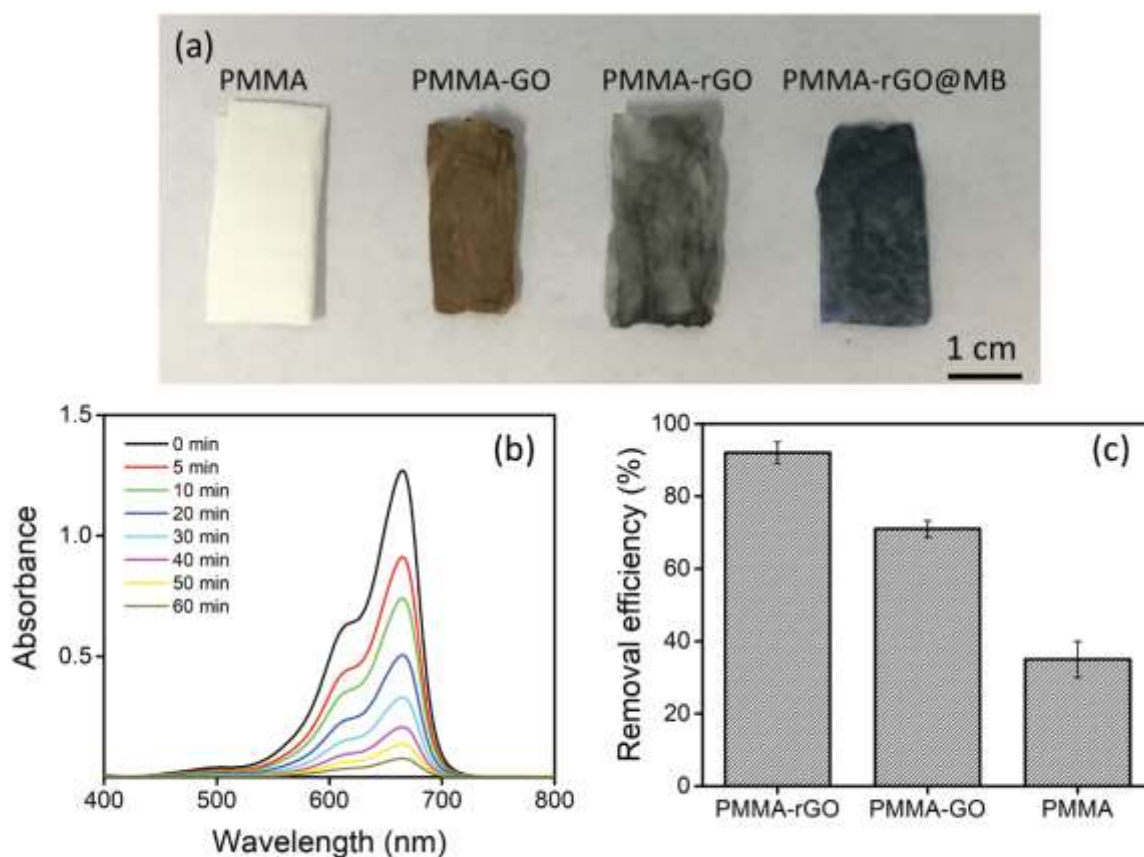


FIGURE 4.4.3: (a) Photographs of PMMA, PMMA-GO, PMMA-rGO and PMMA-rGO@MB nanofiber mats. (b) UV-Vis absorption spectra of MB aqueous solution in the presence of a PMMA-rGO membrane at different time intervals and (c) comparison of the extent of decontamination when using PMMA-rGO, with respect to those obtained with PMMA and PMMA-GO nanofiber mats after 60 min. Error bars indicate the standard deviation of the three measurements. (Reprinted with permission from Mercante *et. al.*¹³⁰)

The high-performance of the PMMA-rGO nanofibers may be ascribed to the following reasons: (1) rGO nanosheets have a large specific surface area and a graphitized basal plane structure, which provide favorable conditions for adsorption. On the other hand, MB has π -electrons arising from C=C, which can easily interact with the π -electrons from the rGO nanosheets. Such π - π interaction of the MB

molecule with rGO nanosheets can be confirmed in the FTIR analysis (Fig. 4.4.2c). After adsorption of MB onto the rGO nanosheets, the peak related to the C=C group presents a blue-shift (now at 1662 cm^{-1}), confirming the adsorption of the MB onto the rGO surface through π - π stacking interactions. In addition, the peak at 1588 cm^{-1} corresponds to the C=S group of the MB dye. Meanwhile, the electrostatic interactions between the positively charged dye and negatively charged residual oxygen-containing functional groups were also reported to play an important role in the adsorption;^{132,149} (2) the large surface area of the PMMA nanofibers could act as spacers and effectively minimize the agglomeration of rGO nanosheets. Also, the tight stacking of nanofibers and planar rGO nanosheets forms a skeleton structure with many pores; (3) the nanofiber structure could also have adsorbed some dye molecules and therefore have a small contribution to the high adsorption performance.

To investigate the detailed adsorption mechanism of the hybrid nanocomposite, we compared the removal efficiency of PMMA-rGO with PMMA-GO as well as with pure PMMA nanofibers. As shown in Fig. 4.3.3c, the enhanced adsorption achieved with the PMMA-rGO nanofibers ($92.0 \pm 2.7\%$) not only significantly decreased with an increase in the number of oxygen groups in the GO nanosheets (PMMA-GO ($71.0 \pm 2.3\%$)), but also dramatically decreased when the pure PMMA nanofibers were used as adsorbent materials ($35.0 \pm 4.9\%$). These results suggest that the superior adsorption capabilities of the rGO-composite nanofibers are due to the synergistic effect of the strong π - π stacking interactions of the exposed reduced graphene nanosheets combined with the properties of the electrospun nanofibers (e.g. high porosity and high-specific surface area per unit mass).

The adsorption kinetics describes the dye adsorption rate and provides valuable data for understanding the controlling mechanism of the adsorption process.¹⁵⁰ Pseudo-first order (eqn (5)) and pseudo-second order (eqn (6)) models, considered as the most matching models to quantify the process of uptake and to study the adsorption kinetics of dyes, were used to evaluate the experimental data.

$$\log(q_e - q_t) = \log q_e - k_1 t \quad (5)$$

$$\frac{t}{q_t} = \frac{1}{k_2 q_e^2} + \frac{t}{q_e} \quad (6)$$

where q_e is the amount of the MB adsorbed at equilibrium (mg g^{-1}), q_t is the amount of dye (mg g^{-1}) adsorbed at time t , while k_1 (min^{-1}) and k^2 ($\text{g mg}^{-1} \text{min}^{-1}$) are the rate constants of the pseudo-second order models, respectively.

The linear fitting results of pseudo-first order ($\log(q_e - q_t)$ vs. t) and pseudo-second order (t/q_t vs. t) models are plotted in Fig. 4.4.4. The correlation coefficient of the pseudo-second order model ($R^2 = 0.994$) is higher than that of the pseudo-first order model ($R^2 = 0.854$), suggesting that chemisorption is the rate-controlling step in the adsorption of MB on the composite nanofiber membrane.¹³¹ This result is in agreement with the kinetic model estimated for aromatic pollutants on GO and rGO adsorbent surfaces.^{38,151}

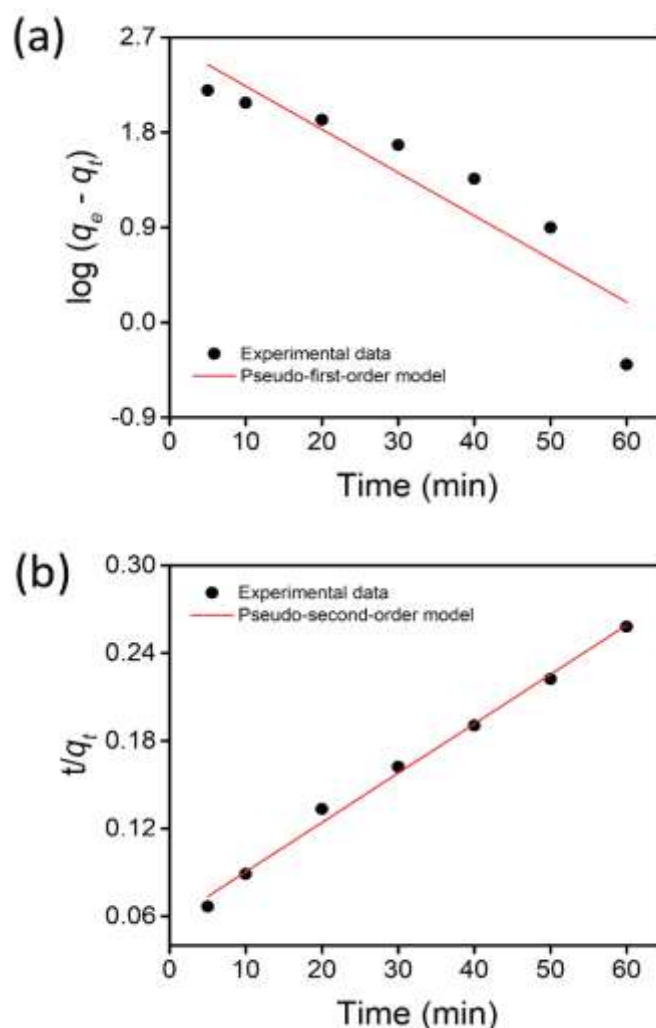


FIGURE 4.4.4: (a) pseudo-first order and (b) pseudo-second order plots for adsorption of MB on PMMA-rGO nanofiber membrane. (Reprinted with permission from Mercante *et. al.*¹³⁰)

To gain insight into the interactive behavior between the adsorbate and adsorbent adsorption, Langmuir and Freundlich isotherm models³⁸ were applied to analyze the equilibrium data, according to eqn (5) and (6), respectively.

$$\frac{C_e}{q_e} = \frac{C_e}{q_{max}} + \frac{1}{q_{max}k_L} \quad (7)$$

$$\ln q_e = \ln k_F + \frac{1}{n} \ln C_e \quad (8)$$

where C_e is the equilibrium concentration (mg L^{-1}) of the MB, q_{max} (mg g^{-1}) is the maximum adsorption capacity, k_L (L mg^{-1}) is the Langmuir constant related to the energy of adsorption and k_F and n are Freundlich constants related to the adsorption capacity and intensity of the adsorbent, respectively.¹⁵²

Figure 4.4.5 depicts the adsorption isotherm for the PMMA-rGO membrane based on the above linear Langmuir (Fig. 4.4.5a) and Freundlich (Fig. 4.4.5b) models, respectively. It is clear that the Langmuir model is reasonable in interpreting the experimental data with R^2 being greater than 0.995, with respect to 0.968 obtained from the Freundlich model. This indicates that the adsorption process is mainly driven by monolayer adsorption and is relatively homogeneous. The Langmuir model is usually based on the assumption of homogeneous adsorption, *i.e.*, equally available sorption sites, monolayer surface coverage, and no interactions between adsorbed species. The maximum adsorption capacity (q_{max}) of MB on the composite nanofiber membrane obtained from the Langmuir isotherm model is 698.51 mg g^{-1} , which is comparatively higher than some of the values reported for other graphene-based adsorbents (see Table 4.1), proving that the PMMA-rGO composite nanofiber membrane is an efficient adsorbent to remove cationic dyes from aqueous solutions.

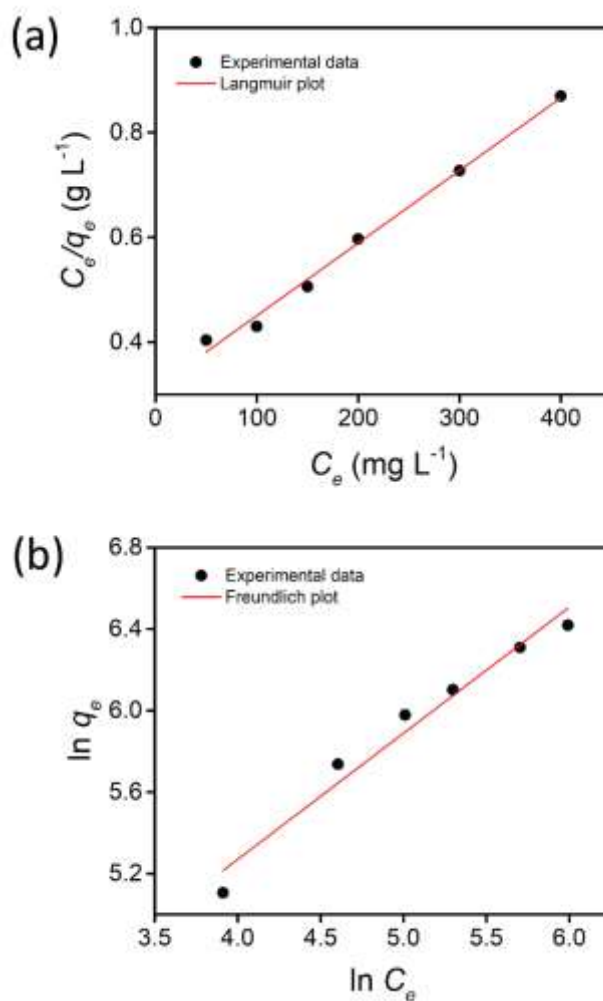


FIGURE 4.4.5: The linearized (a) Langmuir and (b) Freundlich isotherms for adsorption of MB on PMMA-rGO nanofiber membrane. (Reprinted with permission from Mercante *et. al.*¹³⁰)

Table 4.1: Maximum adsorption capacities (q_m) of various graphene-based adsorbents towards MB.

Adsorbent	q_m (mg g ⁻¹)	Reference
Polysaccharide-modified GO composite	769.23	131
GO-polyacrylamide	292.84	137
Agar-GO composite aerogel	578.03	38
GO	714	153
GO-polydamine-PSPSH ^a composite	279.57	154
Cellulose-GO fibers	480.77	155
PMMA-rGO SBS fibers	698.51	This work

^aPoly(Sodium pstyrenesulphonate)

4.5. Conclusion

An easy and efficient methodology using solution blow spinning was employed to fabricate PMMA nanofiber membranes modified with reduced graphene oxide. The developed sorbent membrane was capable of adsorbing MB dye pollutants with a decoloration percentage approaching 92% within 60 min. The high adsorption performance towards MB was mainly attributed to the large surface area of rGO as well as the π - π stacking between the dye pollutant and the rGO nanosheets. The adsorption kinetics follows the pseudo-second order model and the MB adsorption isotherms on PMMA-rGO membranes can be well-fitted with the Langmuir model. The maximum adsorption capacity (q_{max}) is 698.51 mg g⁻¹, which is much higher than that of some other graphene-based adsorbents and electrospun fiber adsorbents. The efficient adsorption capacity towards dye removal is due to the unique rGO properties and to the specific surface area of the composite spun membranes. In comparison with other composite adsorbents, the preparation process of present composite membranes is eco-friendly and facile to operate and regulate, which demonstrates the potential to large-scale applications. Additionally, the methodology can be extended for applications in the remediation of other charged dye contaminants or toxic heavy metal ions.

5. General Conclusions and Future Perspectives

The work described in this dissertation demonstrated that graphene-based materials can be successfully employed in distinct applications due to their several interesting characteristics. Graphene-materials was obtained through the synthesis of graphene oxide and its further reduction showed to be an accessible and suitable way once it does not require sophisticated equipment and complex steps, besides allowing the combination with other materials. Here, graphene was used in two different environmental applications and a few remarks about the results obtained should be highlighted:

- The use of rGO as a component in the sensing units of the e-tongue provided platforms with high conductivity, chemical stability, low electrical noise and oxygen-containing groups in the surface that acts like active sites in pesticide detection;

- The combination of rGO with other materials that also present good electrical conductivity and high specific surface area gave rise to distinct architectures that are simultaneously sensitive to the analytes. The synergistic effect of rGO, conducting polymers and gold nanoparticles resulted in different electrical responses and consequently in a unique fingerprint for each sample, allowing the detection of OPs pesticides at low concentrations;

- Mixtures of OPs pesticides was able to be discriminated by the e-tongue, in which the concentration of one pesticide is directly related to the value of the PC component;

- The combination of nanofibers and rGO provided a composite membrane with desired characteristics for adsorption applications, such as high porosity and high specific surface area;

- The main driving force for the adsorption of the MB was found to be the π - π stacking interactions between rGO and the dye, enabling the achievement of high adsorption performance.

In terms of future work, the results here obtained indicate that graphene can be more exploited as a component in electronic tongues and also in electrochemical sensors. Also, the use of other materials in association with graphene, as well as other structures of graphene-based materials are still to be investigated to further increase their technological applicability.

6. References

1. Bhushan, B. *Springer Handbook of Nanotechnology*. (2010).
2. Poole, C. P. & Owens, F. J. *Introduction to Nanotechnology*. John Wiley & Sons, Inc. **1**, (2003).
3. Hanemann, T. & Szabó, D. V. Polymer-nanoparticle composites: From synthesis to modern applications. *Materials (Basel)*. **3**, 3468–3517 (2010).
4. Geim, A. K. & Novoselov, K. S. The rise of graphene. *Nat. Mater.* **6**, 183–191 (2007).
5. Novoselov, K. S. *et al.* Electric Field Effect in Atomically Thin Carbon Films. *Science (80-.)*. **306**, 666–669 (2004).
6. Novoselov, K. S. *et al.* Two-dimensional atomic crystals. *Proc. Natl. Acad. Sci.* **102**, 10451–10453 (2005).
7. Novoselov, K. S. *et al.* A roadmap for graphene. *Nature* **490**, 192–200 (2012).
8. Whitener, K. E. & Sheehan, P. E. Graphene synthesis. *Diam. Relat. Mater.* **46**, 25–34 (2014).
9. Ciesielski, A. & Samorì, P. Graphene via sonication assisted liquid-phase exfoliation. *Chem. Soc. Rev.* **43**, 381–398 (2014).
10. Pei, S. & Cheng, H. M. The reduction of graphene oxide. *Carbon N. Y.* **50**, 3210–3228 (2012).
11. Stankovich, S. *et al.* Synthesis of graphene-based nanosheets via chemical reduction of exfoliated graphite oxide. *Carbon N. Y.* **45**, 1558–1565 (2007).
12. Glover, A. J., Cai, M., Overdeep, K. R., Kranbuehl, D. E. & Schniepp, H. C. In situ reduction of graphene oxide in polymers. *Macromolecules* **44**, 9821–9829 (2011).
13. Yu, X., Zhang, W., Zhang, P. & Su, Z. Fabrication technologies and sensing applications of graphene-based composite films: Advances and challenges. *Biosens. Bioelectron.* **89**, 72–84 (2017).
14. Poh, H. L. *et al.* Graphenes prepared by Staudenmaier, Hofmann and Hummers methods with consequent thermal exfoliation exhibit very different electrochemical properties. *Nanoscale* **4**, 3515–3522 (2012).
15. Botas, C. *et al.* Graphene materials with different structures prepared from the same graphite by the Hummers and Brodie methods. *Carbon N. Y.* **65**, 156–164 (2013).
16. Hummers, W. S. & Offeman, R. E. Preparation of Graphitic Oxide. *J. Am. Chem. Soc.* **80**, 1339–1339 (1958).
17. Chen, J., Yao, B., Li, C. & Shi, G. An improved Hummers method for eco-friendly synthesis of graphene oxide. *Carbon N. Y.* **64**, 225–229 (2013).
18. Georgakilas, V. *et al.* Functionalization of Graphene: Covalent and Non-Covalent Approaches, Derivatives and Applications. *Chem. Rev.* **112**, 6156–6214 (2012).
19. Compton, O. C. & Nguyen, S. T. Graphene oxide, highly reduced graphene

- oxide, and graphene: Versatile building blocks for carbon-based materials. *Small* **6**, 711–723 (2010).
20. Mao, S., Pu, H. & Chen, J. Graphene oxide and its reduction: modeling and experimental progress. *RSC Adv.* **2**, 2643–2662 (2012).
 21. Chua, C. K. & Pumera, M. Chemical reduction of graphene oxide: a synthetic chemistry viewpoint. *Chem. Soc. Rev.* **43**, 291–312 (2014).
 22. Kuila, T. *et al.* Chemical functionalization of graphene and its applications. *Prog. Mater. Sci.* **57**, 1061–1105 (2012).
 23. Georgakilas, V. *et al.* Noncovalent Functionalization of Graphene and Graphene Oxide for Energy Materials, Biosensing, Catalytic, and Biomedical Applications. *Chem. Rev.* **116**, 5464–5519 (2016).
 24. Layek, R. K. & Nandi, A. K. A review on synthesis and properties of polymer functionalized graphene. *Polym. (United Kingdom)* **54**, 5087–5103 (2013).
 25. Potts, J. R., Dreyer, D. R., Bielawski, C. W. & Ruoff, R. S. Graphene-based polymer nanocomposites. *Polymer (Guildf).* **52**, 5–25 (2011).
 26. Kuilla, T. *et al.* Recent advances in graphene based polymer composites. *Prog. Polym. Sci.* **35**, 1350–1375 (2010).
 27. Zhang, M., Li, Y., Su, Z. & Wei, G. Recent advances in the synthesis and applications of graphene–polymer nanocomposites. *Polym. Chem.* **6**, 6107–6124 (2015).
 28. Guo, Y. *et al.* One pot preparation of reduced graphene oxide (RGO) or Au (Ag) nanoparticle-RGO hybrids using chitosan as a reducing and stabilizing agent and their use in methanol electrooxidation. *Carbon N. Y.* **50**, 2513–2523 (2012).
 29. Zhao, S. *et al.* Three-dimensional graphene/Pt nanoparticle composites as freestanding anode for enhancing performance of microbial fuel cells. *Sci. Adv.* **1**, 1–8 (2015).
 30. Pasricha, R., Gupta, S. & Srivastava, A. K. A Facile and Novel Synthesis of Ag-Graphene-Based Nanocomposites. *Small* **5**, 2253–2259 (2009).
 31. Yin, H. *et al.* Three-dimensional graphene/metal oxide nanoparticle hybrids for high-performance capacitive deionization of saline water. *Adv. Mater.* **25**, 6270–6276 (2013).
 32. Li, L. L. *et al.* Fabrication of graphene-quantum dots composites for sensitive electrogenerated chemiluminescence immunosensing. *Adv. Funct. Mater.* **21**, 869–878 (2011).
 33. Geng, X. *et al.* Aqueous-processable noncovalent chemically converted graphene-quantum dot composites for flexible and transparent optoelectronic films. *Adv. Mater.* **22**, 638–642 (2010).
 34. Pumera, M. Graphene in biosensing. *Mater. Today* **14**, 308–315 (2011).
 35. Perreault, F., Fonseca de Faria, A. & Elimelech, M. Environmental applications of graphene-based nanomaterials. *Chem. Soc. Rev.* **44**, 5861–5896 (2015).
 36. Gautam, M. & Jayatissa, A. H. Ammonia gas sensing behavior of graphene surface decorated with gold nanoparticles. *Solid. State. Electron.* **78**, 159–165 (2012).

37. Santhosh, C. *et al.* Role of nanomaterials in water treatment applications: A review. *Chemical Engineering Journal* **306**, 1116–1137 (2016).
38. Chen, L. *et al.* High performance agar/graphene oxide composite aerogel for methylene blue removal. *Carbohydr. Polym.* **155**, 345–353 (2017).
39. Gerard, M., Chaubey, A. & Malhotra, B. D. Application of conducting polymers to biosensors. *Biosens. Bioelectron.* **17**, 345–359 (2002).
40. Shirakawa, H. & Ieda, S. I. Cyclotrimerization of Acetylene by the Tris(acetylacetonato)titanium(III)-Diethylaluminum Chloride System. *J. Polym. Sci. Polym. Chem.* **12**, 929–937 (1974).
41. Chiang, C. K. *et al.* Electrical Conductivity in Doped Polyacetylene. *Phys. Rev. Lett.* **39**, 1098–1101 (1977).
42. Eftekhari, A. *Nanostructured Conductive Polymers.* (2010).
43. Correa, D. S., Medeiros, E. S., Oliveira, J. E., Paterno, L. G. & Mattoso, L. H. C. Nanostructured Conjugated Polymers in Chemical Sensors: Synthesis, Properties and Applications. *J. Nanosci. Nanotechnol.* **14**, 1–19 (2014).
44. Lange, U., Roznyatovskaya, N. V. & Mirsky, V. M. Conducting polymers in chemical sensors and arrays. *Anal. Chim. Acta* **614**, 1–26 (2008).
45. Lin, W., Chang, H. & Wu, R. Applied novel sensing material graphene/polypyrrole for humidity sensor. *Sensors Actuators B Chem. Chem.* **181**, 326–331 (2013).
46. Xu, C., Sun, J. & Gao, L. Synthesis of novel hierarchical graphene/polypyrrole nanosheet composites and their superior electrochemical performance. *J. Mater. Chem.* **21**, 11253 (2011).
47. Fan, X., Yang, Z. & He, N. Hierarchical nanostructured polypyrrole/graphene composites as supercapacitor electrode. *RSC Adv.* **5**, 15096–15102 (2015).
48. Yang, W. *et al.* Flexible conducting polymer/reduced graphene oxide films: synthesis, characterization, and electrochemical performance. *Nanoscale Res. Lett.* **10**, 222 (2015).
49. Yoo, D., Kim, J. & Kim, J. H. Direct synthesis of highly conductive poly(3,4-ethylenedioxythiophene):Poly(4-styrenesulfonate) (PEDOT:PSS)/graphene composites and their applications in energy harvesting systems. *Nano Res.* **7**, 717–730 (2014).
50. Trusovas, R. *et al.* Recent Advances in Laser Utilization in the Chemical Modification of Graphene Oxide and Its Applications. *Adv. Opt. Mater.* **4**, 37–65 (2016).
51. Legin, A., Rudnitskaya, A. & Vlasov, Y. Electronic Tongues: Sensors, Systems, Applications. *Sensors Updat.* **10**, 143–188 (2002).
52. Vlasov, Y., Legin, A., Rudnitskaya, A., Di Natale, C. & D'Amico, A. Nonspecific sensor arrays ('electronic tongue') for chemical analysis of liquids (IUPAC Technical Report). *Pure Appl. Chem.* **77**, 1965–1983 (2005).
53. Escuder-Gilabert, L. & Peris, M. Review: Highlights in recent applications of electronic tongues in food analysis. *Anal. Chim. Acta* **665**, 15–25 (2010).
54. Riul, A., Dantas, C. a R., Miyazaki, C. M. & Oliveira, O. N. Recent advances in electronic tongues. *Analyst* **135**, 2481–2495 (2010).

55. De Queiroz, D. P. *et al.* The use of an e-tongue for discriminating ethanol/water mixtures and determination of their water content. *Sensors Actuators, B Chem.* **230**, 566–570 (2016).
56. Mercante, L. A. *et al.* Electronic Tongue Based on Nanostructured Hybrid Films of Gold Nanoparticles and Phthalocyanines for Milk Analysis. *J. Nanomater.* **2015**, 1–7 (2015).
57. Ciosek, P. & Wróblewski, W. Sensor arrays for liquid sensing – electronic tongue systems. *Analyst* **132**, 963–978 (2007).
58. Riul, A. *et al.* An electronic tongue using polypyrrole and polyaniline. *Synth. Met.* **132**, 109–116 (2003).
59. Riul, A. *et al.* Artificial taste sensor: Efficient combination of sensors made from Langmuir-Blodgett films of conducting polymers and a ruthenium complex and self-assembled films of an azobenzene-containing polymer. *Langmuir* **18**, 239–245 (2002).
60. Ringner, M. What is principal component analysis? *Nat. Biotechnol.* **26**, 303–304 (2008).
61. Wold, S. Principal Component Analysis. *Chemom. Intell. Lab. Syst.* **2**, 37–52 (1987).
62. Riul, A., Malmegrim, R. R., Fonseca, F. J. & Mattoso, L. H. C. Nano-assembled films for taste sensor application. *Artif. Organs* **27**, 469–472 (2003).
63. Riul, A., Malmegrim, R. R., Fonseca, F. J. & Mattoso, L. H. C. An artificial taste sensor based on conducting polymers. *Biosens. Bioelectron.* **18**, 1365–1369 (2003).
64. Daikuzono, C. M. *et al.* Microfluidic electronic tongue. *Sensors Actuators, B Chem.* **207**, 1129–1135 (2015).
65. Borato, C. E., Riul Jr, A., Ferreira, M., Oliveira Jr, O. N. & Mattoso, L. H. C. Exploiting the Versatility of Taste Sensors Based on Impedance Spectroscopy. *Instrum. Sci. Technol.* **32**, 21–30 (2004).
66. Correa, D. S., Mercante, L. A., Schneider, R., Facure, M. H. M. & Locilento, D. A. in *Handbook of Ecomaterials* 1–29 (2018).
67. Ali, I. & Gupta, V. K. Advances in water treatment by adsorption technology. *Nat. Protoc.* **1**, 2661–2667 (2007).
68. Dabrowski, A. Adsorption - from theory to practice. *Adv. Colloid Interface Sci.* **93**, 135–224 (2001).
69. Largitte, L. & Pasquier, R. A review of the kinetics adsorption models and their application to the adsorption of lead by an activated carbon. *Chem. Eng. Res. Des.* **109**, 495–504 (2016).
70. *Adsorption Technology: A Step-by-Step Approach to Process Evaluation and Application.* (Marcel Dekker, 1985).
71. Do, D. D. *Adsorption Analysis: Equilibria and Kinetics.* (Imperial College Press, 1998).
72. Kenry & Lim, C. T. Beyond the current state of the syntheses and applications of nanofiber technology. *Prog. Polym. Sci.* **70**, 1–17 (2017).

73. Oliveira, J. E., Mattoso, L. H. C., Orts, W. J. & Medeiros, E. S. Structural and morphological characterization of micro and nanofibers produced by electrospinning and solution blow spinning: A comparative study. *Adv. Mater. Sci. Eng.* **2013**, (2013).
74. Medeiros, E. S., Glenn, G. M., Klamczynski, A. P., Orts, W. J. & Mattoso, L. H. C. Solution Blow Spinning: A New Method to Produce Micro- and Nanofibers from Polymer Solutions. *J. Appl. Polym. Sci.* **113**, 2322–2330 (2009).
75. Stojanovska, E. *et al.* A review on non-electro nanofibre spinning techniques. *RSC Adv.* **6**, 83783–83801 (2016).
76. Daristotle, J. L., Behrens, A. M., Sandler, A. D. & Kofinas, P. A Review of the Fundamental Principles and Applications of Solution Blow Spinning. *ACS Appl. Mater. Interfaces* **8**, 34951–34963 (2016).
77. Oliveira, J. E., Mattoso, L. H. C., Medeiros, E. S. & Zucolotto, V. Poly(lactic acid)/carbon nanotube fibers as novel platforms for glucose biosensors. *Biosensors* **2**, 70–82 (2012).
78. Oliveira, J. E. *et al.* Sensor array for water analysis based on interdigitated electrodes modified with fiber films of poly(lactic acid)/multiwalled carbon nanotubes. *IEEE Sens. J.* **13**, 759–766 (2013).
79. Oliveira, J. E. *et al.* Development of poly(lactic acid) nanostructured membranes for the controlled delivery of progesterone to livestock animals. *Mater. Sci. Eng. C* **33**, 844–849 (2013).
80. Ren, J. *et al.* Preparation of polyaniline-coated polyacrylonitrile fiber mats and their application to Cr(VI) removal. *Synth. Met.* **222**, 255–266 (2016).
81. Kampalanonwat, P. & Supaphol, P. Preparation and Adsorption Behavior of Aminated Electrospun Polyacrylonitrile Nanofiber Mats for Heavy Metal Ion Removal. *ACS Appl. Mater. Interfaces* **2**, 3619–3627 (2010).
82. Bode-aluko, C. A., Perea, O., Ndayambaje, G. & Petrik, L. Adsorption of Toxic Metals on Modified Polyacrylonitrile Nanofibres: A Review. *Water, Air, Soil Pollut.* **228**, 1–11 (2017).
83. Roque, A. P. *et al.* Fluorescent PMMA/MEH-PPV electrospun nanofibers: Investigation of morphology, solvent, and surfactant effect. *J. Polym. Sci. Part B Polym. Phys.* **52**, 1388–1394 (2014).
84. Facure, M. H. M., Mercante, L. A., Mattoso, L. H. C. & Correa, D. S. Detection of trace levels of organophosphate pesticides using an electronic tongue based on graphene hybrid nanocomposites. *Talanta* **167**, 59–66 (2017).
85. Briceño, G. *et al.* Increased diazinon hydrolysis to 2-isopropyl-6-methyl-4-pyrimidinol in liquid medium by a specific *Streptomyces* mixed culture. *Chemosphere* **156**, 195–203 (2016).
86. Dominguez, R. B., Alonso, G. A., Muñoz, R., Hayat, A. & Marty, J. L. Design of a novel magnetic particles based electrochemical biosensor for organophosphate insecticide detection in flow injection analysis. *Sensors Actuators B Chem.* **208**, 491–496 (2015).
87. Ho, Y. M., Tsoi, Y. K. & Leung, K. S. Y. Highly sensitive and selective organophosphate screening in twelve commodities of fruits, vegetables and herbal medicines by dispersive liquid-liquid microextraction. *Anal. Chim. Acta*

- 775**, 58–66 (2013).
88. Mehta, J. *et al.* Graphene modified screen printed immunosensor for highly sensitive detection of parathion. *Biosens. Bioelectron.* **83**, 339–346 (2016).
 89. Gong, J., Miao, X., Zhou, T. & Zhang, L. An enzymeless organophosphate pesticide sensor using Au nanoparticle-decorated graphene hybrid nanosheet as solid-phase extraction. *Talanta* **85**, 1344–1349 (2011).
 90. Mishra, R. K., Alonso, G. A., Istamboulie, G., Bhand, S. & Marty, J. L. Automated flow based biosensor for quantification of binary organophosphates mixture in milk using artificial neural network. *Sensors Actuators B Chem.* **208**, 228–237 (2015).
 91. Nunes, G. S. *et al.* Design of a macroalgae amperometric biosensor; application to the rapid monitoring of organophosphate insecticides in an agroecosystem. *Chemosphere* **111**, 623–630 (2014).
 92. Yang, L. *et al.* Determination of 49 organophosphorus pesticide residues and their metabolites in fish, egg, and milk by dual gas chromatography-dual pulse flame photometric detection with gel permeation chromatography cleanup. *J. Agric. Food Chem.* **60**, 1906–1913 (2012).
 93. Obare, S. O. *et al.* Fluorescent chemosensors for toxic organophosphorus pesticides: A review. *Sensors* **10**, 7018–7043 (2010).
 94. Pinheiro, A. de S., da Rocha, G. O. & De Andrade, J. B. A SDME/GC-MS methodology for determination of organophosphate and pyrethroid pesticides in water. *Microchem. J.* **99**, 303–308 (2011).
 95. Liang, P., Guo, L., Liu, Y., Liu, S. & Zhang, T. Z. Application of liquid-phase microextraction for the determination of phoxim in water samples by high performance liquid chromatography with diode array detector. *Microchem. J.* **80**, 19–23 (2005).
 96. Ferrer, C. *et al.* Determination of pesticide residues in olives and olive oil by matrix solid-phase dispersion followed by gas chromatography/mass spectrometry and liquid chromatography/tandem mass spectrometry. *J. Chromatogr. A* **1069**, 183–194 (2005).
 97. Cortina, M., Del Valle, M. & Marty, J. L. Electronic tongue using an enzyme inhibition biosensor array for the resolution of pesticide mixtures. *Electroanalysis* **20**, 54–60 (2008).
 98. Alonso, G. A., Muñoz, R. & Marty, J.-L. Automatic Electronic Tongue for On-Line Detection and Quantification of Organophosphorus and Carbamate Pesticides Using Enzymatic Screen Printed Biosensors. *Anal. Lett.* **46**, 1743–1757 (2013).
 99. Braga, G. S., Paterno, L. G. & Fonseca, F. J. Performance of an electronic tongue during monitoring 2-methylisoborneol and geosmin in water samples. *Sensors Actuators, B Chem.* **171–172**, 181–189 (2012).
 100. Manzoli, A. *et al.* Layer-by-layer fabrication of AgCl–PANI hybrid nanocomposite films for electronic tongues. *Phys. Chem. Chem. Phys.* **16**, 24275–24281 (2014).
 101. Aragay, G., Pino, F. & Merkoçi, A. Nanomaterials for sensing and destroying pesticides. *Chem. Rev.* **112**, 5317–5338 (2012).
 102. Wu, S. *et al.* Electrochemically reduced graphene oxide and Nafion nanocomposite for ultralow potential detection of organophosphate pesticide.

- Sensors Actuators B Chem.* **177**, 724–729 (2013).
103. Scida, K., Stege, P. W., Haby, G., Messina, G. A. & García, C. D. Recent applications of carbon-based nanomaterials in analytical chemistry: Critical review. *Anal. Chim. Acta* **691**, 6–17 (2011).
 104. Pei, H. *et al.* A Graphene-Based Sensor Array for High-Precision and Adaptive Target Identification with Ensemble Aptamers. *J. Am. Chem. Soc.* **134**, 13843–13849 (2012).
 105. Stankovich, S. *et al.* Graphene-based composite materials. *Nature* **442**, 282–286 (2006).
 106. Pumera, M. Graphene-based nanomaterials and their electrochemistry. *Chem. Soc. Rev.* **39**, 4146–57 (2010).
 107. Jiang, H. Chemical preparation of graphene-based nanomaterials and their applications in chemical and biological sensors. *Small* **7**, 2413–2427 (2011).
 108. Pérez-López, B. & Merkoçi, A. Carbon nanotubes and graphene in analytical sciences. *Microchim. Acta* **179**, 1–16 (2012).
 109. Cao, X., Ye, Y. & Liu, S. Gold nanoparticle-based signal amplification for biosensing. *Anal. Biochem.* **417**, 1–16 (2011).
 110. Rivadeneyra, A. *et al.* A novel electrode structure compared with interdigitated electrodes as capacitive sensor. *Sensors Actuators, B Chem.* **204**, 552–560 (2014).
 111. Kumar, G. G. *et al.* Synthesis, Structural, and Morphological Characterizations of Reduced Graphene Oxide-Supported Polypyrrole Anode Catalysts for Improved Microbial Fuel Cell Performances. *ACS Sustain. Chem. Eng.* **2**, 2283–2290 (2014).
 112. Park, B. *et al.* Neutral, Polaron and Bipolaron States in PEDOT Prepared by Photo-electrochemical Polymerization and the Effect on Charge Generation Mechanism in the Solid State Dye Sensitized Solar Cell. *J. Phys. Chem. C* **117**, 22484–22491 (2013).
 113. Tian, Z. Q., Jiang, S. P., Liu, Z. & Li, L. Polyelectrolyte-stabilized Pt nanoparticles as new electrocatalysts for low temperature fuel cells. *Electrochem. commun.* **9**, 1613–1618 (2007).
 114. Haiss, W., Thanh, N. T. K., Aveyard, J. & Fernig, D. G. Determination of Size and Concentration of Gold Nanoparticles from UV-Vis Spectra. *Anal. Chem.* **79**, 4215–4221 (2007).
 115. Fernández-Merino, M. J. *et al.* Vitamin C Is an Ideal Substitute for Hydrazine in the Reduction of Graphene Oxide Suspensions. *J. Phys. Chem. C* **114**, 6426–6432 (2010).
 116. Wang, A. *et al.* Supercapacitors based on highly dispersed polypyrrole-reduced graphene oxide composite with a folded surface. *Appl. Phys. A Mater. Sci. Process.* **120**, 693–698 (2015).
 117. Goncalves, G. *et al.* Surface modification of graphene nanosheets with gold nanoparticles: The role of oxygen moieties at graphene surface on gold nucleation and growth. *Chem. Mater.* **21**, 4796–4802 (2009).
 118. Oliveira, J. E., Scagion, V. P., Grassi, V., Correa, D. S. & Mattoso, L. H. C.

- Modification of electrospun nylon nanofibers using layer-by-layer films for application in flow injection electronic tongue: Detection of paraoxon pesticide in corn crop. *Sensors Actuators, B Chem.* **171–172**, 249–255 (2012).
119. Qualidade de Água. *Resoluções do CONAMA n° 396*, 308–318 (2008).
 120. Varghese, S. S., Lonkar, S., Singh, K. K., Swaminathan, S. & Abdala, A. Recent advances in graphene based gas sensors. *Sensors Actuators B Chem.* **218**, 160–183 (2015).
 121. Robinson, J. T., Perkins, F. K., Snow, E. S., Wei, Z. & Sheehan, P. E. Reduced Graphene Oxide Molecular Sensors. *Nano Lett.* **8**, 3137–3140 (2008).
 122. Lian, W. *et al.* Electrochemical sensor based on gold nanoparticles fabricated molecularly imprinted polymer film at chitosan–platinum nanoparticles/graphene–gold nanoparticles double nanocomposites modified electrode for detection of erythromycin. *Biosens. Bioelectron.* **38**, 163–169 (2012).
 123. Lei, W., Si, W., Xu, Y., Gu, Z. & Hao, Q. Conducting polymer composites with graphene for use in chemical sensors and biosensors. *Microchim. Acta* **181**, 707–722 (2014).
 124. Sun, X., Li, F., Shen, G., Huang, J. & Wang, X. Aptasensor based on the synergistic contributions of chitosan-gold nanoparticles, graphene-gold nanoparticles and multi-walled carbon nanotubes-cobalt phthalocyanine nanocomposites for kanamycin detection. *Analyst* **139**, 299–308 (2014).
 125. Huo, D., Li, Q., Zhang, Y., Hou, C. & Lei, Y. A highly efficient organophosphorus pesticides sensor based on CuO nanowires – SWCNTs hybrid nanocomposite. *Sensors Actuators B Chem.* **199**, 410–417 (2014).
 126. Ebrahim, S. *et al.* Electrochemical sensor based on polyaniline nanofibers/single wall carbon nanotubes composite for detection of malathion. *Synth. Met.* **190**, 13–19 (2014).
 127. Kesik, M. *et al.* An acetylcholinesterase biosensor based on a conducting polymer using multiwalled carbon nanotubes for amperometric detection of organophosphorous pesticides. *Sensors Actuators B Chem.* **205**, 39–49 (2014).
 128. Bakas, I. *et al.* Electrochemical impedimetric sensor based on molecularly imprinted polymers/sol-gel chemistry for methidathion organophosphorous insecticide recognition. *Talanta* **130**, 294–298 (2014).
 129. Valdés-Ramírez, G. *et al.* Automated resolution of dichlorvos and methylparaoxon pesticide mixtures employing a Flow Injection system with an inhibition electronic tongue. *Biosens. Bioelectron.* **24**, 1103–1108 (2009).
 130. Mercante, L. A. *et al.* Solution blow spun PMMA nanofibers wrapped with reduced graphene oxide as efficient dye adsorbent. *New J. Chem.* **41**, 9087–9094 (2017).
 131. Qi, Y., Yang, M., Xu, W., He, S. & Men, Y. Natural polysaccharides-modified graphene oxide for adsorption of organic dyes from aqueous solutions. *J. Colloid Interface Sci.* **486**, 84–96 (2017).
 132. Ramesha, G. K., Vijaya Kumara, A., Muralidhara, H. B. & Sampath, S. Graphene and graphene oxide as effective adsorbents toward anionic and cationic dyes. *J. Colloid Interface Sci.* **361**, 270–277 (2011).

133. Chigome, S., Darko, G. & Torto, N. Electrospun nanofibers as sorbent material for solid phase extraction. *Analyst* **136**, 2879–2889 (2011).
134. Wang, H. *et al.* Three dimensional graphene based materials: Synthesis and applications from energy storage and conversion to electrochemical sensor and environmental remediation. *Adv. Colloid Interface Sci.* **221**, 41–59 (2015).
135. Hadi Najafabadi, H., Irani, M., Roshanfekar Rad, L., Heydari Haratameh, A. & Haririan, I. Removal of Cu 2+ , Pb 2+ and Cr 6+ from aqueous solutions using a chitosan/graphene oxide composite nanofibrous adsorbent. *RSC Adv.* **5**, 16532–16539 (2015).
136. Orozco, J., Mercante, L. A., Pol, R. & Merkoçi, A. Graphene-based Janus micromotors for the dynamic removal of pollutants. *J. Mater. Chem. A* **4**, 3371–3378 (2016).
137. Yang, Y., Song, S. & Zhao, Z. Graphene oxide (GO)/polyacrylamide (PAM) composite hydrogels as efficient cationic dye adsorbents. *Colloids Surfaces A Physicochem. Eng. Asp.* **513**, 315–324 (2017).
138. Li, Y. *et al.* Comparative study of methylene blue dye adsorption onto activated carbon, graphene oxide, and carbon nanotubes. *Chem. Eng. Res. Des.* **91**, 361–368 (2013).
139. Yang, K., Chen, B. & Zhu, L. Graphene-coated materials using silica particles as a framework for highly efficient removal of aromatic pollutants in water. *Sci. Rep.* **5**, 11641 (2015).
140. Farias, R. M. D. C., Menezes, R. R., Oliveira, J. E. & De Medeiros, E. S. Production of submicrometric fibers of mullite by solution blow spinning (SBS). *Mater. Lett.* **149**, 47–49 (2015).
141. Kolbasov, A., Sinha-ray, S., Yarin, A. L. & Pourdeyhimi, B. Heavy metal adsorption on solution-blown biopolymer nano fiber membranes. *J. Memb. Sci.* **530**, 250–263 (2017).
142. Mercante, L. A., Scagion, V. P., Migliorini, F. L., Mattoso, L. H. C. & Correa, D. S. Electrospinning-based (bio)sensors for food and agricultural applications: A review. *TrAC - Trends Anal. Chem.* **91**, 91–103 (2017).
143. Lee, J. S. *et al.* Role of molecular weight of atactic poly(vinyl alcohol) (PVA) in the structure and properties of PVA nanofabric prepared by electrospinning. *J. Appl. Polym. Sci.* **93**, 1638–1646 (2004).
144. Ryu, Y. J., Kim, H. Y., Lee, K. H., Park, H. C. & Lee, D. R. Transport properties of electrospun nylon 6 nonwoven mats. *Eur. Polym. J.* **39**, 1883–1889 (2003).
145. Bao, Y., Lai, C., Zhu, Z., Fong, H. & Jiang, C. SERS-active silver nanoparticles on electrospun nanofibers facilitated via oxygen plasma etching. *RSC Adv.* **3**, 8998 (2013).
146. Pham, V. H., Dang, T. T., Hur, S. H., Kim, E. J. & Chung, J. S. Highly conductive poly (methyl methacrylate)(PMMA)-reduced graphene oxide composite prepared by self-assembly of PMMA latex and graphene oxide through electrostatic interaction. *ACS Appl. Mater. Interfaces* **4**, 2630–2636 (2012).
147. Wang, F., Duan, L., Wang, F. & Chen, W. Environmental reduction of carbon nanomaterials affects their capabilities to accumulate aromatic compounds. *NanoImpact* **1**, 21–28 (2016).

148. Thakur, V. K., Vennerberg, D., Madbouly, S. A. & Kessler, M. R. Bio-inspired green surface functionalization of PMMA for multifunctional capacitors. *RSC Adv.* **4**, 6677 (2014).
149. Bai, S. *et al.* One-pot solvothermal preparation of magnetic reduced graphene oxide-ferrite hybrids for organic dye removal. *Carbon N. Y.* **50**, 2337–2346 (2012).
150. Patel, S. & Hota, G. Iron oxide nanoparticles immobilized PAN nanofibers: Synthesis and adsorption studies. *RSC Adv.* **6**, 15402–15414 (2016).
151. Zhang, X. *et al.* Interactions between Antibiotics and Graphene-Based Materials in Water: A Comparative Experimental and Theoretical Investigation. *ACS Appl. Mater. Interfaces* **8**, 24273–24280 (2016).
152. Wu, Z. *et al.* Enhanced adsorptive removal of p-nitrophenol from water by aluminum metal–organic framework/reduced graphene oxide composite. *Sci. Rep.* **6**, 25638 (2016).
153. Yang, S. T. *et al.* Removal of methylene blue from aqueous solution by graphene oxide. *J. Colloid Interface Sci.* **359**, 24–29 (2011).
154. Wan, Q. *et al.* Facile and highly efficient fabrication of graphene oxide-based polymer nanocomposites through mussel-inspired chemistry and their environmental pollutant removal application. *J. Mater. Sci.* **52**, 504–518 (2017).
155. Chen, L. *et al.* Removal of methylene blue from water by cellulose/graphene oxide fibres. *J. Exp. Nanosci.* **11**, 1156–1170 (2016).

Appendix A

Supporting Information of Chapter I



Figure A1: Digital picture (A) and a scheme of the geometrical features of the IDE (B). The fingers have a length (L) of 4 mm and width (w) and distance between fingers (s) of 10 μm .

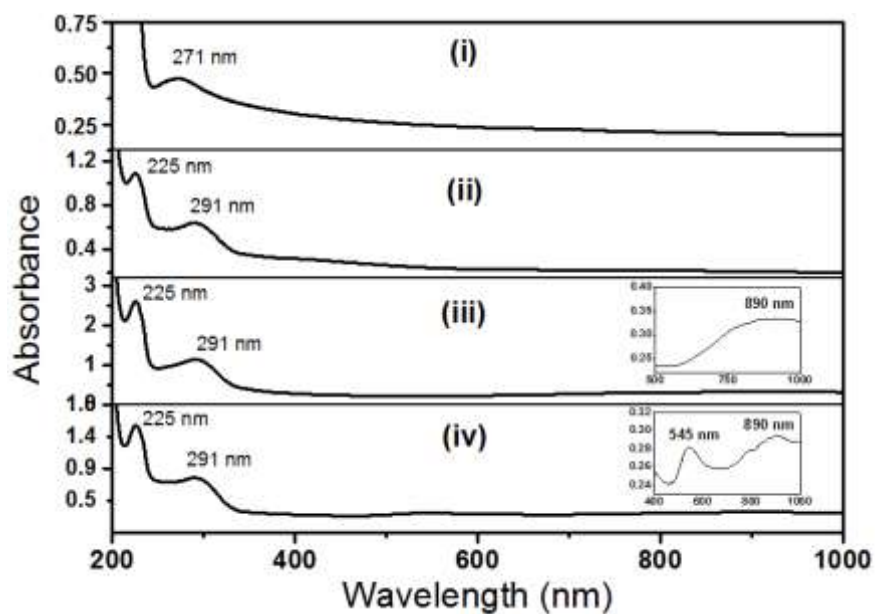


Figure A2: UV-Vis absorption spectra of: (i) rGO, (ii) PPy-rGO, (iii) PEDOT:PSS-rGO and (iv) PEDOT:PSS-rGO-AuNPs.

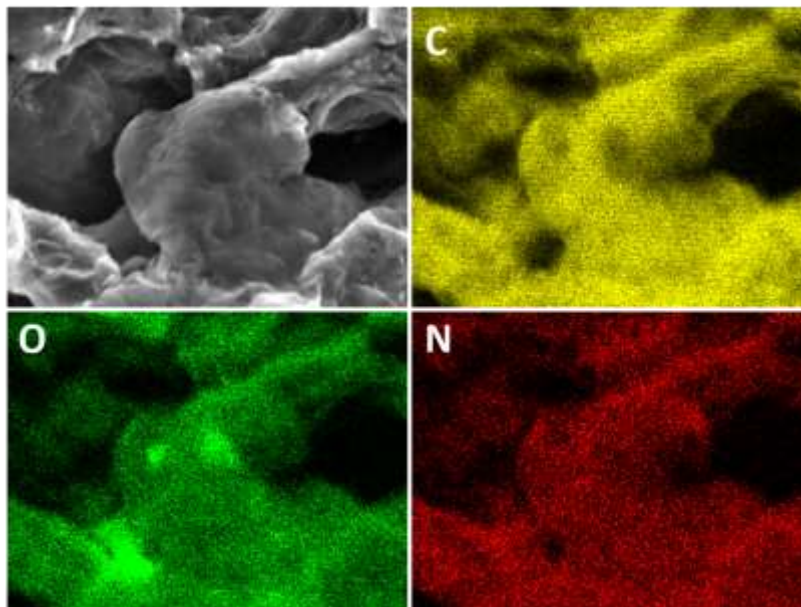


Figure A3: Energy-dispersive X-ray (EDX) spectroscopy images illustrating the distribution of the C, O and N elements in the PPY-rGO nanocomposite.

Appendix B

Supporting Information of Chapter II

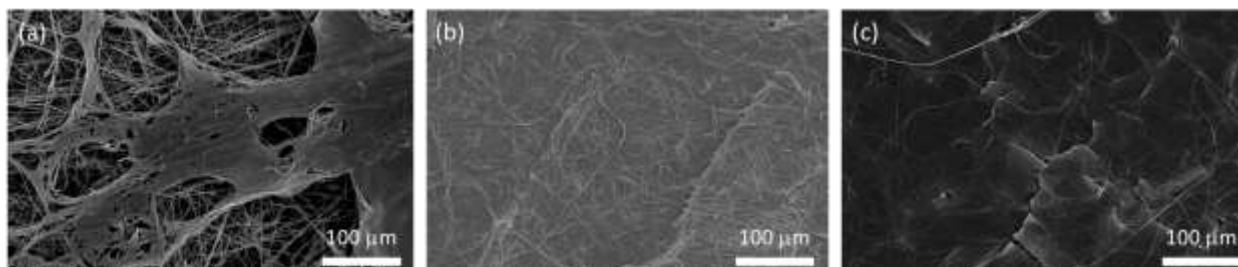


Figure B1: SEM images of PMMA-GO nanofibers using distinct adsorption times: (a) 30 min, (b) 1h and (c) 2h.

Appendix C

Publication rights permission



Copyright
Clearance
Center

RightsLink[®]

Home

Create Account

Help

✉



Title: Detection of trace levels of organophosphate pesticides using an electronic tongue based on graphene hybrid nanocomposites

Author: Murilo H.M. Facure, Luiza A. Mercante, Luiz H.C. Mattoso, Daniel S. Correa

Publication: Talanta

Publisher: Elsevier

Date: 15 May 2017

© 2017 Elsevier B.V. All rights reserved.

LOGIN

If you're a [copyright.com](https://www.copyright.com) user, you can login to RightsLink using your [copyright.com](https://www.copyright.com) credentials. Already a [RightsLink](https://www.rightslink.com) user or want to [learn more?](#)

Please note that, as the author of this Elsevier article, you retain the right to include it in a thesis or dissertation, provided it is not published commercially. Permission is not required, but please ensure that you reference the journal as the original source. For more information on this and on your other retained rights, please visit: <https://www.elsevier.com/about/our-business/policies/copyright#Author-rights>

Figure C1: Permission to use the article “Detection of trace levels of organophosphate pesticides using an electronic tongue based on graphene hybrid nanocomposites”.

Solution blow spun PMMA nanofibers wrapped with reduced graphene oxide as an efficient dye adsorbent

L. A. Mercante, M. H. M. Facure, D. A. Locilento, R. C. Sanfelice, F. L. Migliorini, L. H. C. Mattoso and D. S. Correa, *New J. Chem.*, 2017, **41**, 9087
DOI: 10.1039/C7NJ01703K

If you are the author of this article you do not need to formally request permission to reproduce figures, diagrams etc. contained in this article in third party publications or in a thesis or dissertation provided that the correct acknowledgement is given with the reproduced material.

If you are the author of this article you still need to obtain permission to reproduce the whole article in a third party publication with the exception of reproduction of the whole article in a thesis or dissertation.

Figure C2: Permission to use the article "Solution blow spun PMMA nanofibers wrapped with reduced graphene oxide as an efficient dye adsorbent".

**SPRINGER NATURE LICENSE
TERMS AND CONDITIONS**

Jan 25, 2018

This Agreement between Mr. Murilo Henrique Moreira Facure ("You") and Springer Nature ("Springer Nature") consists of your license details and the terms and conditions provided by Springer Nature and Copyright Clearance Center.

License Number	4276051327905
License date	Jan 25, 2018
Licensed Content Publisher	Springer Nature
Licensed Content Publication	Nature Materials
Licensed Content Title	The rise of graphene
Licensed Content Author	A. K. Geim, K. S. Novoselov
Licensed Content Date	Mar 1, 2007
Licensed Content Volume	6
Licensed Content Issue	3
Type of Use	Thesis/Dissertation

Figure C3: Permission to use figures from the article "The rise of graphene".

**JOHN WILEY AND SONS LICENSE
TERMS AND CONDITIONS**

Jan 25, 2018

This Agreement between Mr. Murilo Henrique Moreira Facure ("You") and John Wiley and Sons ("John Wiley and Sons") consists of your license details and the terms and conditions provided by John Wiley and Sons and Copyright Clearance Center.

License Number	4276050639774
License date	Jan 25, 2018
Licensed Content Publisher	John Wiley and Sons
Licensed Content Publication	Small
Licensed Content Title	Graphene Oxide, Highly Reduced Graphene Oxide, and Graphene: Versatile Building Blocks for Carbon-Based Materials
Licensed Content Author	Owen C. Compton, Son Binh T. Nguyen
Licensed Content Date	Mar 11, 2010
Licensed Content Pages	13
Type of use	Dissertation/Thesis

Figure C4: Permission to use figures from the article "Graphene Oxide, Highly Reduced Graphene Oxide, and Graphene: Versatile Building Blocks for Carbon-Based Materials".

**ROYAL SOCIETY OF CHEMISTRY LICENSE
TERMS AND CONDITIONS**

Jan 25, 2018

This Agreement between Mr. Murilo Henrique Moreira Facure ("You") and Royal Society of Chemistry ("Royal Society of Chemistry") consists of your license details and the terms and conditions provided by Royal Society of Chemistry and Copyright Clearance Center.

License Number	4276060315681
License date	Jan 25, 2018
Licensed Content Publisher	Royal Society of Chemistry
Licensed Content Publication	Analyst
Licensed Content Title	Recent advances in electronic tongues
Licensed Content Author	Antonio Riul Jr., Cléber A. R. Dantas, Celina M. Miyazaki, Osvaldo N. Oliveira Jr.
Licensed Content Date	Aug 20, 2010
Licensed Content Volume	135
Licensed Content Issue	10
Type of Use	Thesis/Dissertation

Figure C5: Permission to use figures from the article "Recent advances in electronic tongues".